The Heart and a Fibrotic Interstitium

By

Vivian Sagvaag

Thesis for the Master degree in

Experimental and Human Physiology

University of Bergen

Department of Biomedicine

2009

Acknowledgements

This Master's thesis was carried out at the Department of Physiology, Institute of Biomedicine, University of Bergen, during the period August 2008 to June 2009.

First and foremost I would like to thank my supervisors, 1.amenuensis Anne Kristine Jonassen, and Rolf Kåre Reed, for all the help and support given throughout this project, and not least for introducing me to a fascination cardiovascular research field.

I would also like to thank my colleagues at the Cardiac Research Unit for providing a positive working atmosphere, being great supporters and always very helpful. Bert-Inge Rosengren should be acknowledged his guidance through hydroxyproline analysis. Extra gratitude should also be given to Erik Helgeland, providing us with surgical guidance and PowerLab setup, and Sigurd Danielsen, for taking superb photographs during the *in vivo* protocols. Moreover, Eva-Katrine Aarnes, Lars Breivik and Maren Askeland should be thanked, for reading through preliminary parts of my thesis.

Black zone would have been pretty lonesome without Mira Mykletun, my Tivoli radio and P3. Thank you Mira, for joining me through ups and downs, during pulmonary artery ruptures, anaesthetic overdoses and not least the experience of managing to wake rats up from surgery.

Furthermore, the past year would not have been the same without my fellow students in the reading room, especially Charlotte, Maren and Mira for all the great lunch breaks we have had.

Last, but not least, I would like to mention my family and friends for supporting-, encouraging-, and believing in me.

Bergen, 29.05.09

Vivian Sagvaag

Table of Contents

Abstract

Background: Several acute and chronic diseases disposes for myocardial oedema and fibrosis, leading to impaired cardiac function, presumably as a result of an increased chamber stiffness. Mechanisms and adverse effects of both oedema and fibrosis in the heart have only partly been elucidated; however, the temporal and spatial development is still unknown.

Objective: The purpose of our study was to: (1) establish an *in vivo* pulmonary artery (PA) banded model that produces myocardial oedema and fibrosis in both ventricles, and (2) examine the temporal and spatial development of oedema- and subsequent fibrosis formation in both acute and chronic protocols.

Methods: A PA-banded model was utilized to elevate the right ventricular (RV) pressure, to subsequently produce both right- and left sided ventricular myocardial oedema and on a longer time scale, fibrosis, in male Wistar rats. The left ventricular (LV) oedema formed due to the drainage system via sinus venosus and the thebesian veins, further exacerbated by lymphatic congestion, allowed us to study the LV itself without interferences from manipulation. Gravimetric wet to dry weight ratio as an index of total tissue water (TTW) and oedema, and hydroxyproline as an indicator of total collagen synthesis and fibrosis formation, were measured in the RV and LV and the septum.

Results: Right ventricular developed pressure (RVDP) was significantly elevated in all PA-banded procedures as compared the initial pressure measurements pre-PA-banding and the corresponding sham values. Contraction (dP/dt maximum) and relaxation (dP/dt minimum) of the RV pressure was increased in both acute and chronic experimental PA-banded groups, while heart rate (HR) remained unchanged. No significant increases in TTW or total collagen content was seen until 17 days post-PA-banding (note: n=1 in each group).

Conclusions: Continuously increased RV pressures post-PA-banding demonstrated a marked response to the constriction. The heart seemed to overcome the elevated pressure by increasing cardiac contraction and relaxation (dP/dt). No indication of myocardial oedema or fibrosis formation was seen within the first hour of acute PA-banding. Preliminary data from chronic protocols indicated that myocardial oedema was not developed within 24 hours, but after 17 days post-PA-banding, with subsequent increases in collagen synthesis (note: n=1 in each group).

1 Introduction

1.1 Background

Cardiovascular diseases (CVDs) are a group of disorders of the heart and blood vessels. CVDs are the number one cause of death worldwide, with an estimate of 17 million deaths every year, representing 30% of all global deaths (1, 2). The annual number of deaths from the global epidemic of CVDs is not only increasing, but also shifting from developed to developing nations (3). By 2030, numbers are expected to increase towards 24.2 million deaths, a total of 32.5% of all deaths (3). Norway is a well developed western European country with both high life expectancy and standard of living. CVD incidents are however high, accounting for as much as 35% of all deaths in 2007 (4).

A number of acute and chronic CVDs, such as pulmonary hypertension, chronic pulmonary hypertension with right heart failure, chronic arterial hypertension, cardioplegic arrest, coronary sinus hypertension and myocardial ischemia predisposes for myocardial oedema, i.e. excess of interstitial water, which is associated with impaired heart function (5-10). Chamber stiffness, possibly due to the excess interstitial water and decreased ventricular compliance, seems to be an important contributor to the compromised cardiac performance (11). It has been suggested that oedema formation is a trigger for interstitial fibrosis, i.e. altered interstitial matrix, resulting in an even stiffer myocardium (12), that will further impair cardiac function (13). Collagen, the most abundant constituent of the interstitial matrix, is an important marker of fibrosis formation (13).

A disease situation highly disposed for myocardial oedema and fibrosis formation can be simulated in an experimental model of pulmonary artery (PA) banding, in which the right ventricular (RV) pressure is increased by surgically reducing the diameter of the PA, i.e. the main outgoing artery from the RV (13). Mechanisms and effects of both myocardial oedema and fibrosis have been partly elucidated; however, the temporal- and spatial development of oedema- and fibrosis formation in the heart still needs to be revealed. With a clinical application in mind, knowing the time point and the spatial distribution of oedema- and fibrosis formation in the *in vivo* rat model would be important in the process of finding the most effective time for therapeutic treatment, in addition to answering how optimal administration should be carried out.

1.2 The Normal Interstitium

Interstitial, meaning "in between", refers to the spaces between the capillary wall and the cells. About one-sixth of the body volume is comprised by the interstitial spaces, which mediates the exchange of oxygen, nutrients and waste products between the vascular system and the cells. All organs have an interstitium and the basic structure is similar in all tissue organs, i.e. it is principally organized with the same components. However, the amount of interstitium and also the relative amounts of each structure may differ from organ to organ (14). The following components are regarded as the basic constituents of the interstitial structure:

a) Collagen
b) Glycosaminoglycans (GAGs)
c) Salt solution
d) Proteins derived from plasma

1.2.1 Collagen – The Fibre Framework

Collagen structures predominantly constitute the interstitial skeleton. Because collagens are tensile elements, their main functional effects are to resist changes in tissue configuration and volume. Collagens also function to exclude proteins, and further, they immobilize the glycosaminoglycans (GAGs) of the binding network (15).

Collagens are a group of proteins sharing structural resemblance. To date, there are at least 29 known types (16), divided into several subtypes that are widely expressed throughout the organs and tissues. Collagen molecules are arranged into triple helices. The individual α-chains are left-handed coiled polypeptide chains, each containing ~1000 amino acids, with approximately three residues per turn, every third being glycine (17). Mainly hydroxyproline and proline make up the remaining amino acids in the triplet (17). Three chains are coiled into a right-handed superhelix that is stabilized by hydrogen bonds (interpeptide hydrogen bonding) (17).

Fibril- and subsequent fibre assembly of the collagen molecules are localized to the extracellular space. Collagen is originally synthesized by fibroblast cells that secrete procollagen, a precursor molecule, which has both NH_2- and COOH- terminal non-triple

helical extensions (18, 19). Procollagen is further modified post-translational to give differences in hydroxylation and glucosylation (20). Peptides originating from part of the COOH- and NH_2-terminal cleaved during the post-translational modification act as cellular feedback regulator for the synthesis (21).

1.2.2 Glycosaminoglycans (GAGs) – The Gel Phase

Glycosaminoglycans (GAGs) constitute a main importance of interstitial fluid volume control. They are generally described as linear polymers of disaccharide repeat units consisting of hexosamine and hexuronic acid (22). GAGs are specifically characterized by their content and distribution of charged anionic groups: the carboxylate group (—COO^-), sulphate ester group (—O—SO_3^-) and sulphamino group (—N— SO_3^-) that are fully ionized under physiological conditions (22). The osmotic pressure of GAG solutions is partly or wholly due to a high negative charge density, producing counter ion attraction and a Donnan distribution of diffusible ion density, which refers to the distribution of ion species between two ionic solutions separated by a semipermeable membrane, i.e. the vascular wall. Based on structural similarities, four main GAG families are currently known (23). Subfamilies are differentiated by the different composition of the disaccharide units and the possible positions of substituents (23). Most GAGs are sulphated and found covalently attached as side branches to a protein backbone to form large, brush-shaped proteoglycans (15). However, their major component hyaluronan, is non-sulphated and found as free polymers *in vivo,* structurally unbranched (essentially linear) with a quaternary structure of random coil (15). GAG molecules do not seem to have particularly strong chemical bindings to each other, but show a marked internal entanglement at concentrations >0.1% for hyaluronan and >1% for proteoglycans. At these concentrations, they seem to form a continuous network, possessing a gel-like appearance (15).

1.2.3 The Fluid Compartment

The interstitial fluid compartment is comprised of a salt solution and proteins derived from plasma.

Total body water in an average adult human accounts approximately for 60% of the body weight. This is distributed between the intracellular and extracellular compartments, 40- and 20%, respectively (24). Interstitial fluid makes up more than three fourths of the extracellular fluid, and the remaining one fourth is found in the plasma (24).

Interstitial proteins are the same proteins that are found in the plasma compartment, because of the permeability characteristics of the capillary wall. Water and electrolytes passes, however, much more readily than does plasma proteins, giving the ultrafiltrate a reduced protein content. The interstitial protein concentration is consequently a function of the selectivity of the capillary barrier and the transcapillary fluid flux (14, 25). In the present context, the important property of the interstitial proteins is their colloid osmotic pressure, contributing to the fluid balance by exerting an interstitial suction force.

1.2.4 Transendothelial Transport

Transport across the capillary wall is determined by three important factors:

1. The properties of the capillary membrane
2. The transcapillary hydrostatic pressures
3. The transcapillary osmotic pressures

Capillary blood pressure, i.e. the hydrostatic pressure, is the primary force driving ultrafiltration. Filtration is however opposed by the osmotic pressure of the plasma proteins, which exerts the only absorptive force. Ernest H. Starling described this relationship in 1896, stating that the net capillary filtration will be zero when the transcapillary hydrostatic pressure difference equals the net effective protein osmotic transcapillary pressure (26). Today, the forces and factors determining the transcapillary fluid flux are often referred to as the Starling forces, which are summarized in the Starling equation (Formula 1):

$$J_v = L_pS[(P_c - P_i) - \sigma(COP_p - COP_i)]$$

Formula 1. The Starling equation. J_v equals the transcapillary fluid flux. L_p denotes the hydraulic conductance and S the surface area of the capillary wall. P and COP are hydrostatic and colloid osmotic pressures, and subscrips c, p and i denote capillary, plasma and interstitial, respectively. σ is the reflection coefficient.

In addition to the forces exerted, filtration highly depends on the capillary filtration coefficient (CFC), namely the product of the hydraulic conductance (L_p) and the surface area of the capillary wall (S). The reflection coefficient (σ) is defined as the ratio of the observed to theoretical colloid osmotic pressure across the membrane, which denotes the degree of protein leakage across a semipermeable membrane (25). An illustration of the interplay between the various factors determining fluid exchange is shown below (Figure 1).

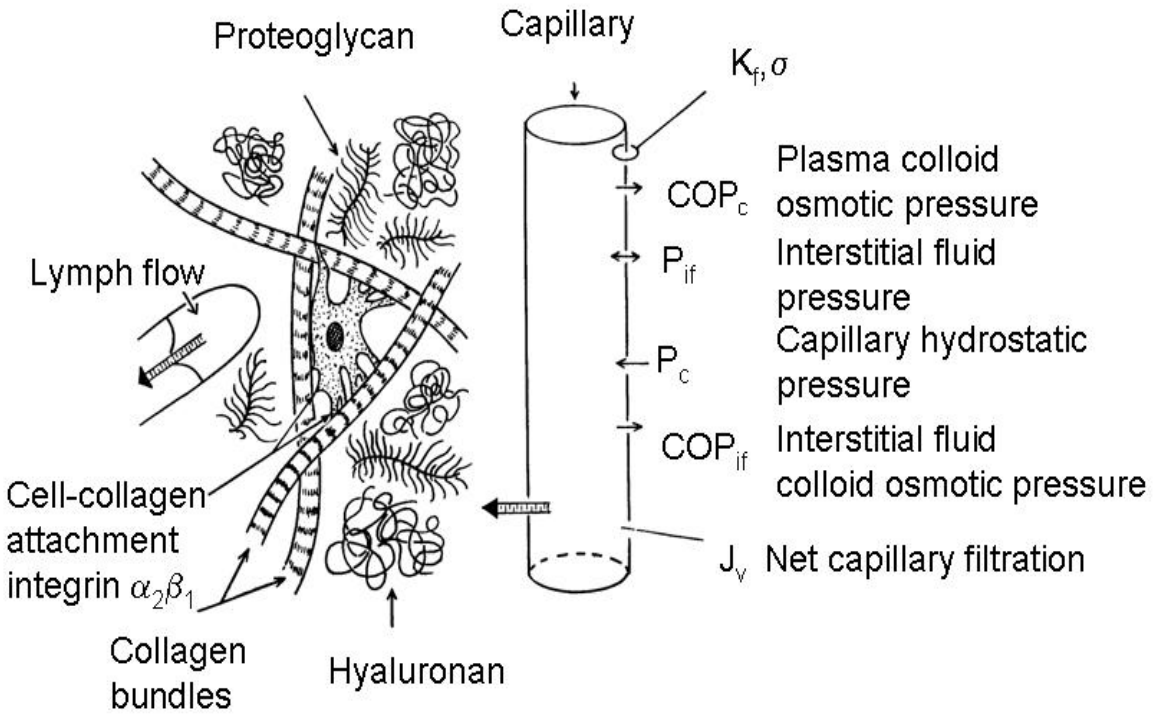

Figure 1. Schematic overview of the normal interstitial space including its most important constituents and the transcapillary interstitial fluid exchange system. The interstitial skeleton is mainly made up by collagen bundles. Proteoglycans represents the multiple sulphated glycosaminoglycan (GAG) chains, anchored to a linear core protein, whereas the long hyaluronans represent the non-sulphated GAGs, both having a high negative-charge density that is partly or wholly responsible for the osmotic pressure. Transcapillary fluid exchange is determined by the forces exerted by the capillary and the interstitium (27).

1.3 Oedema Formation

The interstitial volume is to a large extent self-adjusting, due to the interplay of a number of local automatic mechanisms that functionally act as buffers against extracellular volume changes, as described in the next section (Section 1.3.1). However, when these buffer-margins of safety are exceeded, oedema becomes apparent. Oedema is an excess of interstitial fluid, in skin normally representing a doubling of interstitial volume, and will inevitably develop if the capillary filtration rate exceeds the lymphatic drainage rate for a sufficient period of time. Various causes and conditions leading to oedema formation are described in section 1.3.2.

1.3.1 Safety Factors to Prevent Oedema Formation

Under normal circumstances, i.e. in a steady state, the partition of the total extracellular volume (ECV) between plasma and interstitium is governed by the net capillary filtration (J_V) and lymph flow (J_L). A major factor in volume homeostasis is without doubt lymphatic drainage. Although normal filtration fraction is only ~0.2-0.3% (most tissues), 4-8 litres of lymph is produced per day from the more than ~4000 litres of plasma that passes through the human microcirculation over the course of day (25). Interstitial volume is to a large extent self-adjusting, due to a number of local automatic mechanisms. Three consecutive lines of defence against oedema development tend to protect the body against fluid accumulation during acute insults, as indicated schematically in Figure 2 (28). The first mechanism of defence (I) and probably the most important in everyday orthostasis, is an immediate response to increased arterial and/or venous pressure, independent of changes in the interstitial fluid volume (IFV). This response is accounted for by precapillary vasoconstriction (PCC) acting through myogenic and/or a local reflex mechanism that will reduce the capillary filtration coefficient (CFC) and limit the rise in capillary pressure (P_c) and net filtration transcapillary pressure (ΔP_{tc}). The second line of defence (II), activated by the increase of net capillary filtration rate (J_v) and IFV, is accounted for by a rise of interstitial pressure (P_i), dilution of interstitial fluid protein and reduction of its colloid osmotic pressure (COP_i), and increase of local capillary plasma protein concentration and colloid osmotic pressure (COP_p). The third line of defence (III) is lymph flow (J_L), removing fluid and proteins from the interstitium, that will increase in response to a rise in (P_i) (and possibly IFV). Both mechanism II and III

depends on a rise in IFV, and will thus develop more slowly. Also, only mechanisms II and III will be activated in hypoproteinemia, but during a general tendency to oedema formation, the washout of proteins from the interstitium, i.e. the reduction in interstitial protein mass, will also restore and rise intravascular protein mass to maintain COP_p.

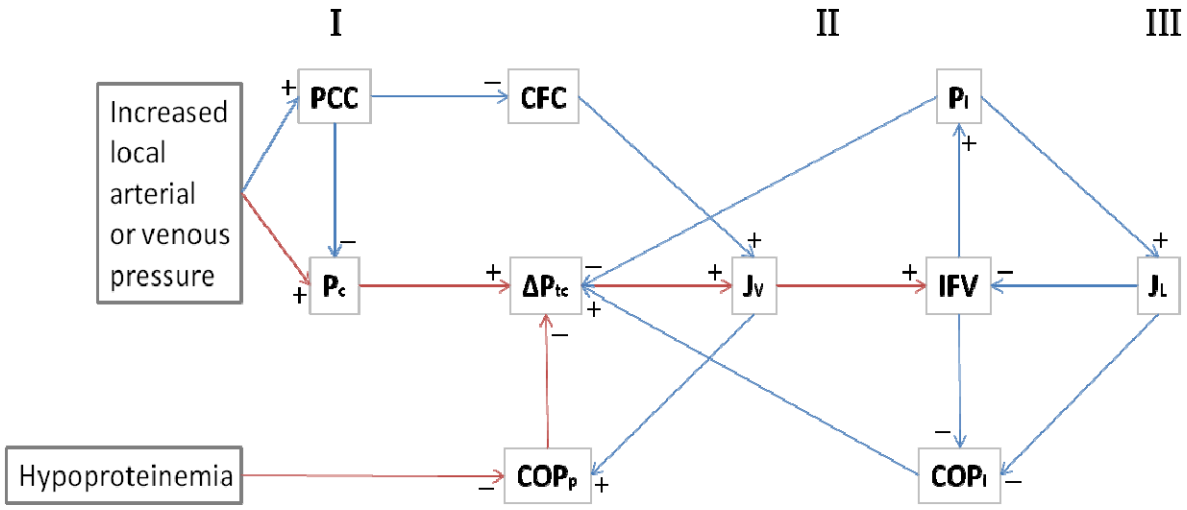

Figure 2. Local mechanisms preventing or limiting a rise in interstitial fluid volume (IFV) and oedema formation at increased local arterial and/or venous pressure and during hypoproteinemia. Three consecutive lines of defence (I, II and III) may be envisioned. Red arrows indicate oedema-provoking sequences, whereas blue arrows indicate oedema-preventing mechanisms. An increase in the parameter at origin of an arrow will increase (+) or reduce (–) the parameter at arrowhead. PCC, precapillary vasoconstriction; CFC, capillary filtration coefficient; P_c, capillary pressure; ΔP_{tc}, net transcapillary filtration pressure; COP_p, colloid osmotic pressure of capillary plasma; J_v, net capillary filtration rate; IFV, interstitial fluid volume; COP_i, colloid osmotic pressure of interstitial fluid; P_i, interstitial fluid pressure; J_L, lymph flow rate. [Modified from Aukland (28)]

In addition to the self-adjustments of the Starling forces, including local vasomotor reactions, and not least the automatic adjustments of the lymph flow, the interstitial structural network plays an important role in preventing oedema formation. A main contributor to this are the naturally rigid collagen fibres that resist changes in tissue configuration and volume (15).

1.3.2 Oedema Provoking Factors

The "safety factors" working as buffers against oedema formation described in section 1.3.1, may be exceeded in various cases of illnesses, leading to imbalanced Starling forces, in which high filtration rates (J_v) or low lymph flow (J_L) give rise to tissue swelling. Capillary pressure (P_c) increase is observed in situations of chronically raised venous pressure, seen in e.g. right ventricular (RV) heart failure arisen from a clinical course of untreated pulmonary arterial hypertension (11). A fall in plasma colloid osmotic pressure (COP_p) can occur in several conditions, such as protein loss from e.g. malabsorption, nephrotic syndrome (protein loss into urine), or reduced protein synthesis originating from e.g. cirrhosis. This reduction will subsequently raise the capillary filtration rate, and may lead to clinical oedema if the concentration falls below ~2g/dL (29). Oedema is one of the cardinal features of inflammation. Inflammation is associated with endothelial gap formation and increased capillary permeability, i.e. hydraulic conductance (L_p) and increased protein permeability, in addition to decreased reflection coefficient (σ) (30). Oedema formation is also enhanced if lymph flow (J_L) is compromised. Sun *et al.* demonstrated that an occlusion of the cardiac lymphatic system produced myocardial oedema within hours of such degree that coronary capillary compression occurred (31).

1.3.3 The Oedematous Heart

Myocardial oedema is a common manifestation of many clinical states, and is known for its negative impact on cardiac function. Fluid accumulation has been demonstrated in a number of acute and chronic conditions, including cardiac transplantation (32), decreased plasma colloid osmotic pressure or myocardial lymph flow impairment during cardioplegia (8, 33), altered microvascular permeability by chronic arterial hypertension (34), elevation of myocardial microvascular pressures (35), sepsis (36), ischemia (5), pulmonary hypertension and right heart disease (6, 7).

Laine and Allen (7) demonstrated a decreased capability of the heart to maintain cardiac output at a constant left atrial pressure as myocardial oedema increased. Chamber stiffness, i.e. end-diastolic pressure-volume relationship, shown to increase with oedema accumulation, seems to be an important contributor to this impaired cardiac function, but through a poorly understood mechanism (37, 38). One consequence of increased myocardial stiffness due to

excess water is decreased ventricular compliance, which in concert with the accumulated water can compromise cardiac ability to contract efficiently (38, 39). Although interstitial collagen has great tensile strength and accounts for a major part of the interstitial structure, increased interstitial volume and pressure may displace the collagen fibres or break collagen struts loose from their anchoring points (40). Because contraction relies on a well-organized interstitial matrix, a disruption in the collagen structure may compromise cardiac function. Additionally, Davis *et al.* demonstrated that myocardial oedema may be a trigger for interstitial fibrosis formation, resulting in increased collagen deposition, also compromising cardiac contraction ability (13). Myocardial oedema as a possible trigger for fibrosis is further described in section 1.4. Figure 3 depicts and summarizes the various factors that enhance myocardial dysfunction due to oedema formation.

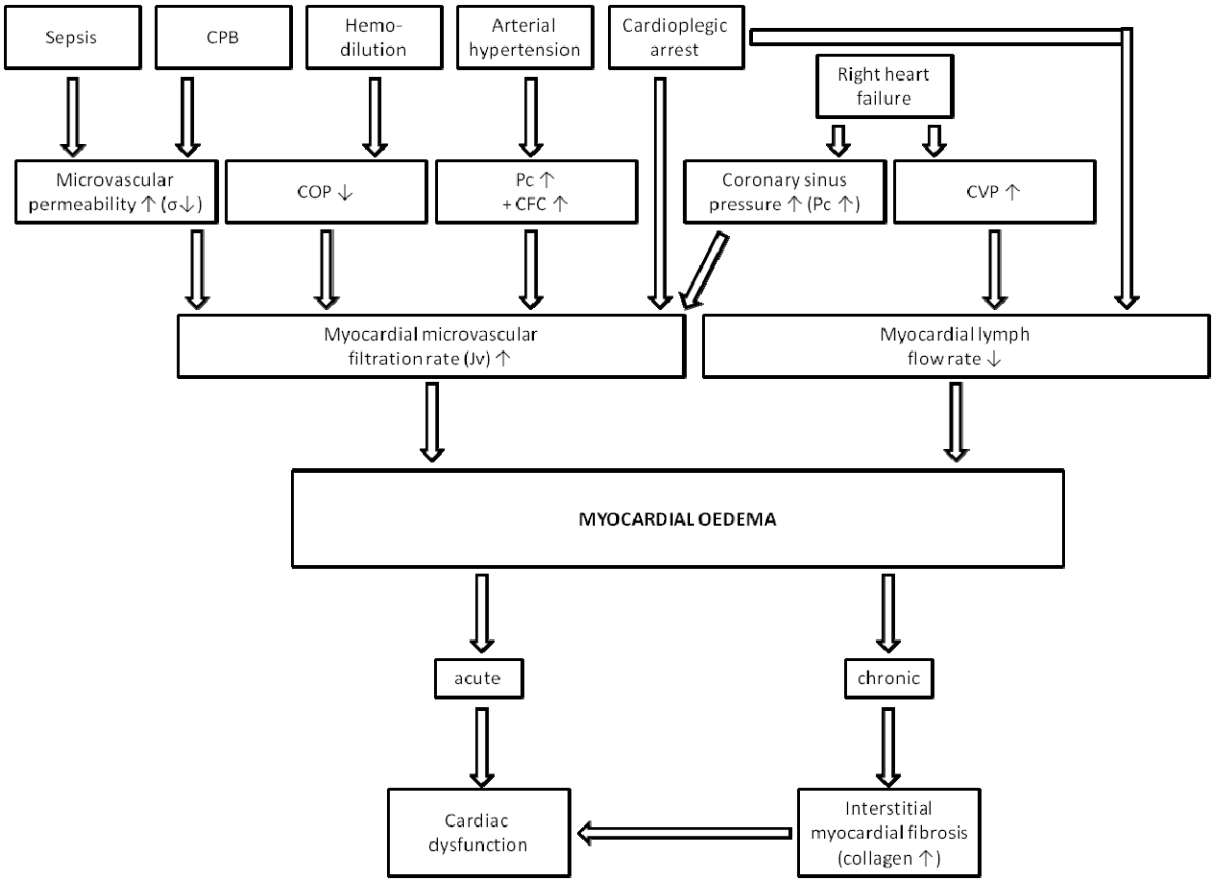

Figure 3. Mechanisms that potentiate myocardial oedema formation. Both chronic and acute formation of myocardial oedema results in a compromised cardiac function. If myocardial oedema persists chronically, subsequent altered myocardial interstitial matrix or fibrosis formation will thus further indirectly depress cardiac function. CPB, cardiopulmonary bypass; COP, colloid osmotic pressure; P_c, capillary pressure; CFC, capillary filtration coefficient; CVP, central venous pressure. [Modified from Mehlhorn *et al.* (10)]

Interstitial myocardial oedema is generally associated with left ventricular (LV) dysfunction. Even right ventricular (RV) heart failure is associated with LV dysfunction, due to the construction and interconnection of the heart ventricles. In an experimental model of pulmonary artery (PA) banding, i.e. surgical reduction of the PA diameter to increase the RV pressure, myocardial oedema has been shown to be induced in both the RV and LV. LV becomes oedematous for two reasons. First, as the PA pressure increases, the right atrial (RA) and RV hydrostatic pressures rises. Pressure subsequently increases in the coronary sinus and thebesian veins that drain into the RA from the LV. The pressure increase disperses further through to the LV, resulting in increased trans-microvascular fluid flux and LV oedema formation. Secondly, as cardiac lymph drains into the central venous system, right-sided pressure elevations (RA, RV, and central-venous pressure) results in a decreased rate of removal of excess fluid from the LV via cardiac lymphatics, thus further exacerbating LV oedema formation (41, 42).

1.4 The Fibrotic Heart Interstitium

Regulation of extracellular matrix protein deposition is an important event in many physiologic- and pathological situations. Disturbances of this tightly regulated balance, for example by myocardial oedema, as demonstrated by Davis *et al.* (13), may lead to fibrosis development, thus, altering structure, architecture and shape of the heart. Fibrotic diseases are characterized by excessive scarring due to vigorous production, deposition and contraction of the extracellular matrix. Collagen is the main protein in the connective tissue, in which excessive deposition is the pathological hallmark of fibrosis. The fibrotic process occurs over time, such as months or years, leading to both diastolic and systolic cardiac dysfunction (43).

The function of fibrosis is not completely known. Normally, collagen networks are thought to be involved in the transmission of force generated in muscle tissue, acting mechanically in synergy with myocytes (12). Unfortunately, excessive deposition of collagen within the myocardium causes a reduced ventricular compliance and cardiac pathology. With the use of Young's modulus for bending of collagen, MacKenna and co-workers demonstrated, and further suggested that the collagen fibres may be major contributors to diastolic stiffness (12).

Within the heart, transforming growth factor-β_1 (TGF-β_1), a pro-fibrotic cytokine and a potent stimulator of collagen-producing fibroblasts, appears to be one of several factors that mediate

fibrosis formation, e.g. Rosenkranz *et al.* showed this in transgenic mice over-expressing TGF-β_1 (44). Angiotensin II (AII) has also been shown to be involved in the regulation of myocardial fibrosis (45). AII seems to be linked to TGF-β_1, in which Campbell *et al.* (46), among others, indicated an up-regulation of TGF-β_1 by AII in myofibroblasts and cardiac fibroblasts. Proteolytic enzymes, such as matrix metalloproteinases (MMPs) play an important role in promoting change and remodelling, and seem to be a large contributor of sustaining a dynamic network within the extracellular matrix. The roles of MMPs and TGF-β_1 in cardiac remodelling may be intertwined. Increasing evidence point towards an MMP regulation by TGF-β_1 as demonstrated among others, by Overall *et al.* (47).

1.5 Aims of Study

Various acute and chronic diseases causes impaired cardiac function as a result of the development of myocardial oedema and fibrosis. The main purpose of this study was to establish an experimental model of pulmonary artery (PA) banding, to investigate the temporal and potentially spatial distributional development of myocardial oedema- and subsequent fibrosis formation in the heart. By banding the PA, the vessel diameter is reduced, resulting in an increased right ventricular (RV) pressure that not only induces myocardial oedema and fibrosis in the RV, but also in the left ventricle (LV). The LV also experiences myocardial oedema since thebesian veins and the sinus venosus together drain the RV and the LV. However, since only the RV experiences a pressure overload, the LV is not subjected to the subsequent hypertrophy. This allows us to study the oedemic- and fibrotic effects in the LV, independent of the pressure load and hypertrophic effects that are found in the RV.

Within this frame of reference the specific aims were:

1. Establish an *in vivo* rat model with PA banding, previously shown by others to induce myocardial oedema in both the right and left heart ventricles (7, 13) with subsequent fibrosis formation (13).

2. Investigate the temporal and spatial development of myocardial oedema, i.e. answering when and where oedema formation takes place, after increasing PA-pressure in an acute (30-/60 minutes of PA-banding) and chronic (24 hours/17 days of PA-banding) experimental situation. This is determined by using a gravimetric wet to dry weight ratio [(Wet weight – Dry weight)/Dry weight)].

3. Examine the temporal fibrosis formation after increasing PA-pressure. This is demonstrated by a quantitative hydroxyproline determination, further correlated to the total collagen content as a fibrotic marker.

2 Materials and Methods

All procedures were approved by and performed in accordance with regulations from the Norwegian Committee for Animal Research (The National Animal Research Authority (FOTS) bearing the project id 1222). The number of animals used was minimized to meet the guidelines from the Ethical Committee.

2.1 Animals

Experiments were performed on 37 adult male Wistar HanTAc:WH rats (Taconic Europe AS, Denmark) weighing between 240g and 380g. Rats were acclimatized for one week before experimental procedures, in accordance with Appendix A of the European Convention (ETS NO. 123) (48). Animals were housed in groups of 3 or 4 prior to the experimental procedures in ventilated Makrolon IVC Type IV cages (Techniplast Gazzada S.a.r.l., Italy) on soft wooden bedding (Scanbur AS Norway, Norway), with 70 air changes/hour. Rats undergoing chronic procedures were, however, allowed to recover individually in separate cages after surgery and stored in a Scantainer (Scanbur AS Norway, Norway). The animals had access to water and were fed a standard diet (MR1/Special Diet Service) *ad libitum*. Ambient temperature in the animal facility was kept within an optimum of 20-21°C, with a relative humidity of 40-60% and an artificial light/dark cycle of 12/12 hours. Health monitoring was performed regularly according to the recommendations of Federation of the European Laboratory Animal Science Associations (FELASA) (49).

2.2 Anaesthesia

Anaesthesia is inevitable in comprehensive surgical procedures. It is strictly necessary to evaluate the anaesthesia of choice in advance, as some anaesthetics may intervene directly or indirectly with your tissue of interest, hence, giving test results with systematic errors. Propofol (PropoVet) with fentanyl-fluanisone (Hypnorm) pre-medication was found to provide stress-free induction, easily controlled anaesthesia, good analgesia and muscle relaxant for the animals during surgery. This anaesthetic combination has previously been shown to provide very stable heart rates, respiration and blood pressures within normotensive limits (50), which made it suitable in our rat model of pulmonary artery (PA) banding for measuring cardiovascular parameters.

2.2.1 Pre-Anaesthetic Care

Animals were anesthetized with a bolus dose, 0.5-1.0mL/kg (to effect), of Hypnorm intraperitoneally (i.p.) (VetPharma Ltd., UK), containing Fentanyl citrate 0.315mg/mL and Fluanisone 10mg/mL. Hypnorm produced heavy sedation and usually unconsciousness in the rats, providing a stress-free environment during the intravenous (i.v.) cannulation of the tail vein. Hypnorm is a neuroleptanalgesic, in which fentanyl is an analgesic of the morphine type and fluanisone is a neuroleptic of the butyrophenone group.

Due to an unfortunate delivery stop from the manufacturer, Hypnorm was temporarily unavailable. Consequently, some animals were anesthetized with a bolus dose of Mebumal (pentobarbital, 50mg/kg, Apotek 1 Svanen, Norway). Mebumal is a short-acting barbiturate derivative, normally used as a sedative in circulatory research, and was given in a dosage of 0.1mL/100g i.p., until anaesthetic level was reached. Similar to Hypnorm, it also provided heavy sedation, giving a less stressful cannulation of the tail vein.

2.2.2 Peri-Anaesthetic Care

PropoVet (propofol, 10mg/mL, Abbott Logistics B.V., Netherlands), given i.v. via the tail vein, provided deep anaesthesia during surgery. Propofol (2,6-diisopropylfenol) is a quick acting and short lasting i.v. anaesthetic with a rapid recovery time (50). It has a depressant effect on the central nervous system (CNS), leading to unconsciousness in the animal. A bolus i.v. dose of 0.1mL was useful in deepening the anaesthesia to a level which could be easily maintained by a continuous infusion, keeping a flow rate of 3-5mL/kg/h (to effect). The appropriate depth of anaesthesia was judged by the absence of eye reflexes and a response to paw pinch.

2.2.3 Post-Anaesthetic Care

Incision area was greased with EMLA cream (AstraZeneca AS, Norway), containing lidocain and prilocain, providing local analgesia. The rats were also treated with 0.05mg/kg s.c. Temgesic (Schering-Plough AS, Norway) repeatedly two to three times a day, till three days after surgery. Temgesic is an analgesic with an action time of 8-12 hours, containing buprenofinhydrochlorid equivalent to 0.3mg of buprenorphine.

2.2.4 Euthanasia

The rat heart was fully exposed during the surgical sternotomical procedure. Methods and analyses in later stages of the research required heart samples, so that animal euthanasia was performed by excision of the rat heart.

2.3 Experimental Setup

2.3.1 Tail Vein Cannulation and Endotracheal Intubation

All surgical procedures were performed under aseptic conditions. Animals were anesthetized as described in section 2.2. Lateral or dorsal tail vein was cannulated using a 24 gauge (G) intravenous (i.v.) cannula (Terumo Europe N.V., Leuven, Belgium). Cannulation was prepared by cleansing the tail with warm water on sterile compresses, followed by thoroughly drying. This preparation both further dilated the veins, and more importantly, cleansed and softened the skin, facilitating insertion. The tail veins are located immediately beneath the skin, and were thus, entered at a very shallow angle, almost parallel to the vein by slightly bending the tail down at the incision area (Figure 4).

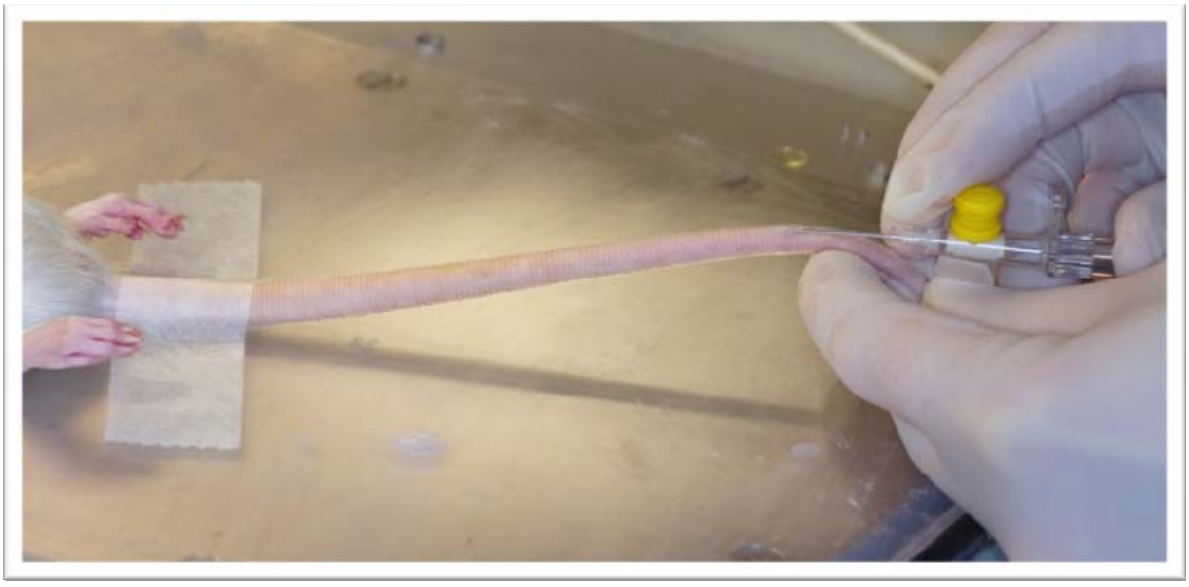

Figure 4. Cannulation of the lateral or dorsal tail vein, using a 24G cannula.

The i.v. cannula was connected to a syringe pump (Terumo terfusion syringe pump TE-312, Vingmed AS, Norway) to provide a continuous infusion of PropoVet (3-5mL/kg/h), as described in section 2.2. The rats were intubated to prevent the lungs from collapsing during the open chested procedure, utilizing the principle of blind oral tracheal intubation as described by Stark *et al.* (51). An over-the-needle 16G i.v. cannula (Becton Dickinson AB, Sweden) was modified to a tube, simply by removing the needle. Intubation was performed

by placing its upper incisors onto a wire construction made on a Plexiglas wall, leaving the rat all stretched (Figure 5). In this way, there was an easy and straight path from the mouth to the trachea. Using a very strong light source onto the throat, shining through the skin, one could easily recognize the larynx when the tongue was withdrawn. The cannula could then be placed into the trachea to ventilate the rat.

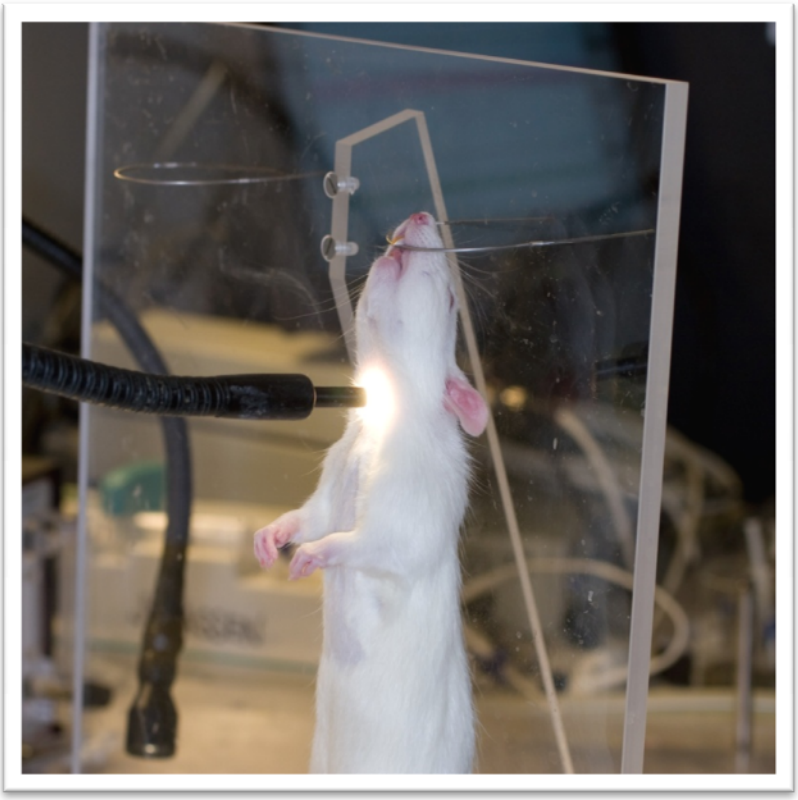

Figure 5. Intubation of rat in order to provide sufficient ventilation while under open thorax surgery. The pathway to the trachea was more easily recognized by placing the upper incisors onto the wire construction while strongly illuminating the throat.

The endotracheal tube was further connected to a mechanical ventilator (TOPO dual mode ventilator, Kent Scientific Corporation, USA) set to deliver room air, and adjusted to a constant volume ventilation mode set to ~50 breaths per minute and a peak inspiratory pressure meter reading a physiologic range between 8 and 12 cmH_2O. Settings were later adjusted in accordance with the measured blood gases to meet optimal ventilation for the rat, keeping pH values within limits of 7.40-7.44. To maintain a positive airway pressure throughout the expiratory phase during the mechanical ventilation, a positive end expiratory pressure (PEEP) was provided, thus keeping alveolar distension, improving pulmonary gas

exchange, and not least, preventing pulmonary oedema. The PEEP was obtained by causing a resistance on the exhaust port of the ventilator. A section of tubing was therefore placed 3.5 cm under water in a filter flask, creating a PEEP of 3.5 cmH_2O (Figure 6).

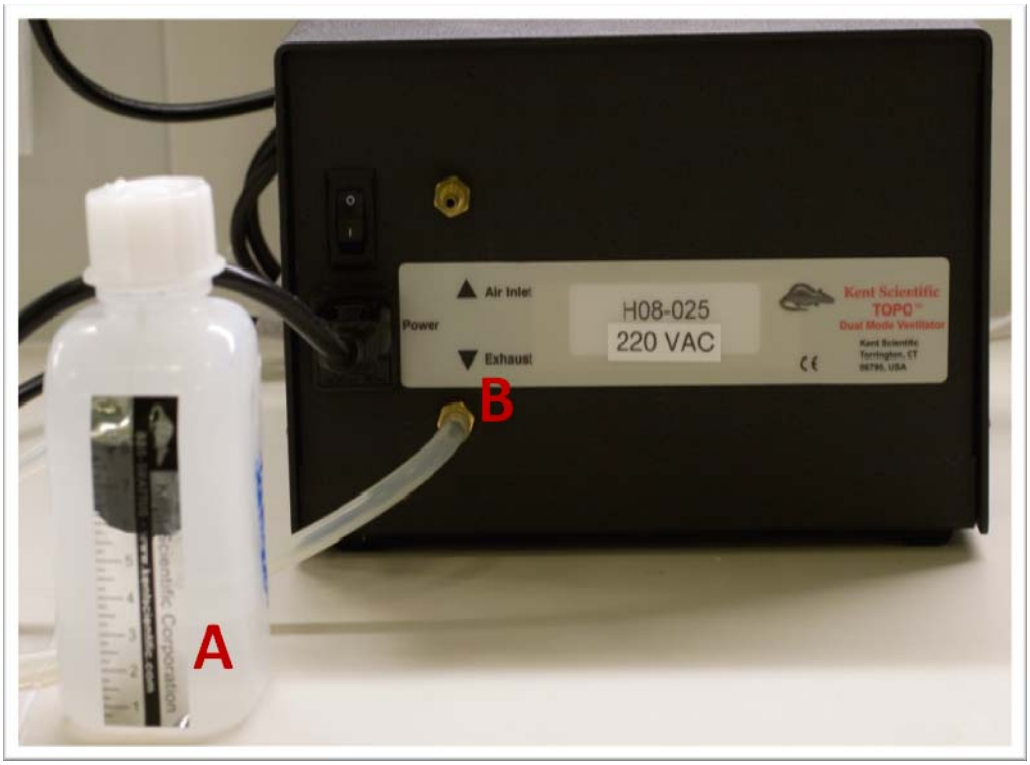

Figure 6. Positive end expiratory pressure (PEEP) setup. A filter flask was filled with 3.5cm of water above the section tube (A) and connected to the exhaust port of the ventilator (B), to create a PEEP of 3.5cmH_2O.

2.3.2 Surgical Procedure – Pulmonary Artery Banding

The intubated rat was placed in a supine position onto a water-circulated operation tablet (Figure 7), maintaining a core body temperature of 37±1°C. Temperature was continuously controlled with a rectal probe (Figure 7). Eyes were treated with eye ointment (Simplex Øyesalve, Ophtha AS, Denmark) to prevent drying during the surgical procedure. Further on, rat chest was shaved and cleansed with alcohol.

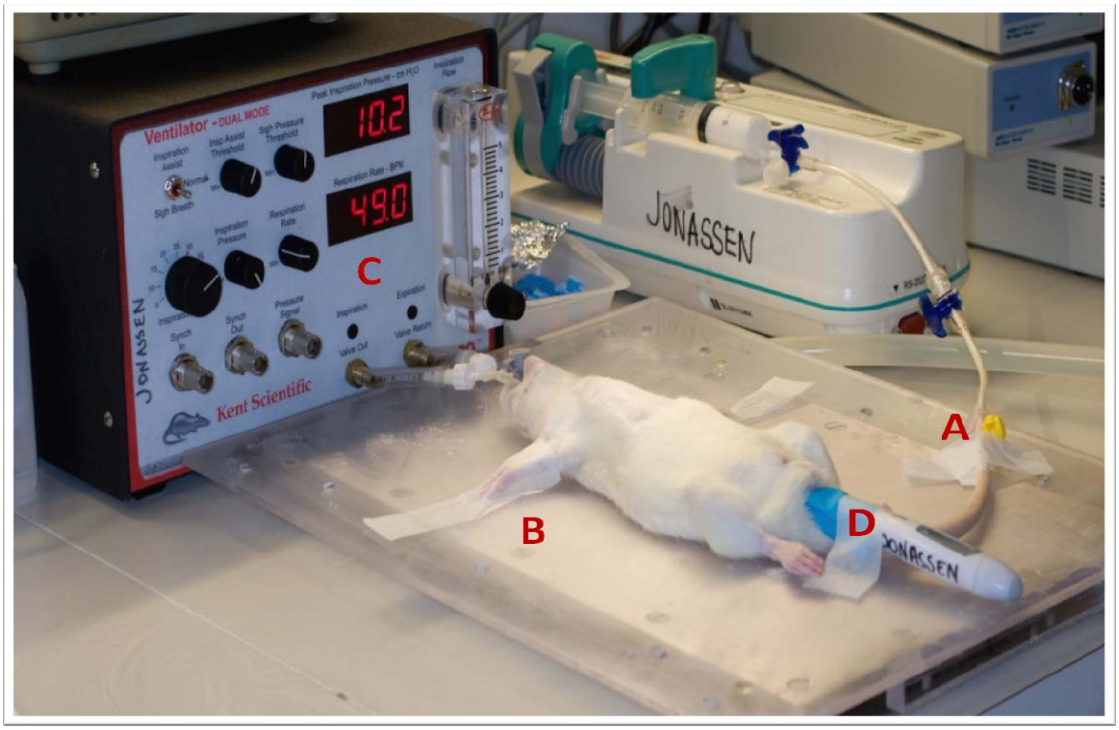

Figure 7. Experimental setup before surgically opening the animals. Anaesthesia was provided through a continuous intravenous (i.v.) infusion via one of the tail veins (A). Anesthetized rats were restrained onto an operating tablet (B). Sufficient ventilation was provided through a tracheal intubation connected to a ventilator (C). A rectal probe continuously controlled the body temperature in the animal (D).

The chest was opened by a median sternotomy to reach the heart that was cradled in the incised pericardium for stabilization. Furthermore, the pulmonary artery (PA) was identified under the thymus and dissected from the surrounding tissue (Figure 8), followed by passing a 4-0 silk suture around (Figure 9). Experimental groups, except sham operated rats, were subsequently treated with the following: The suture was tied tightly against a 16G luer stub

adapter (Figure 10), which was then quickly removed, leaving only the suture around the PA. This procedure produced a PA-constriction of the same diameter in each rat.

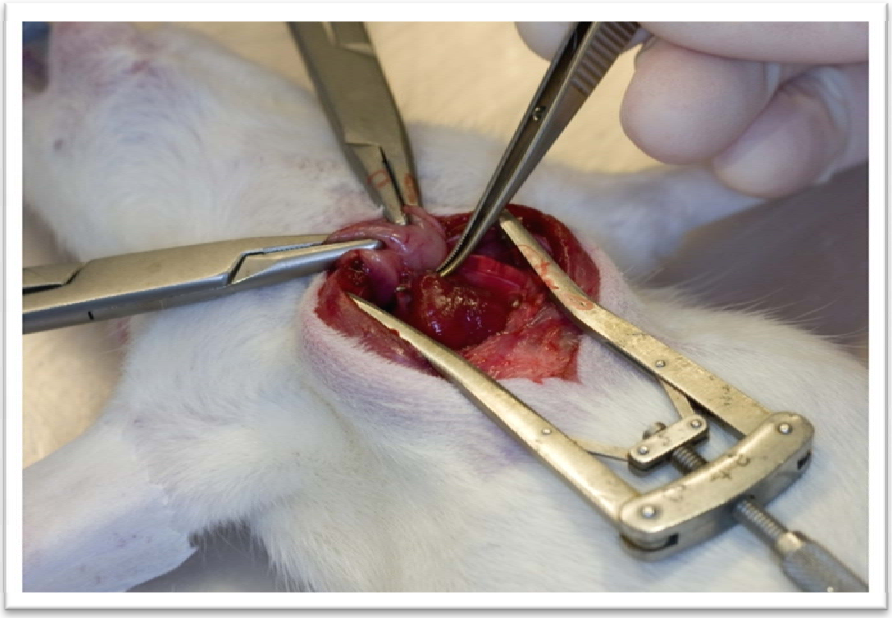

Figure 8. Pulmonary artery (PA) dissection from the surrounding tissue. The heart and PA were accessed via median sternotomy. PA was identified under the thymus and dissected from the surrounding tissue, using surgical forceps.

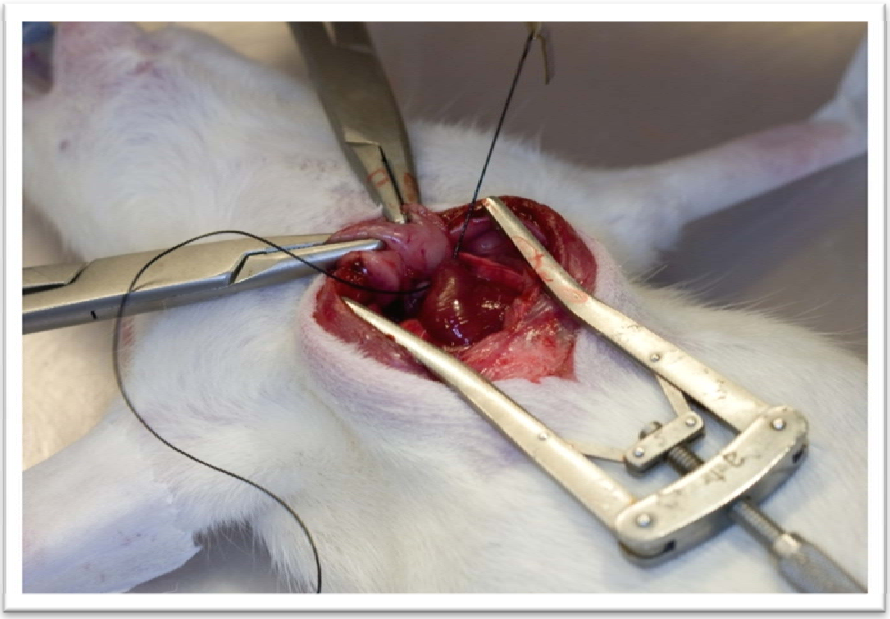

Figure 9. Preparation for pulmonary artery (PA) banding. A 4-0 silk suture was placed around the PA, now ready for banding.

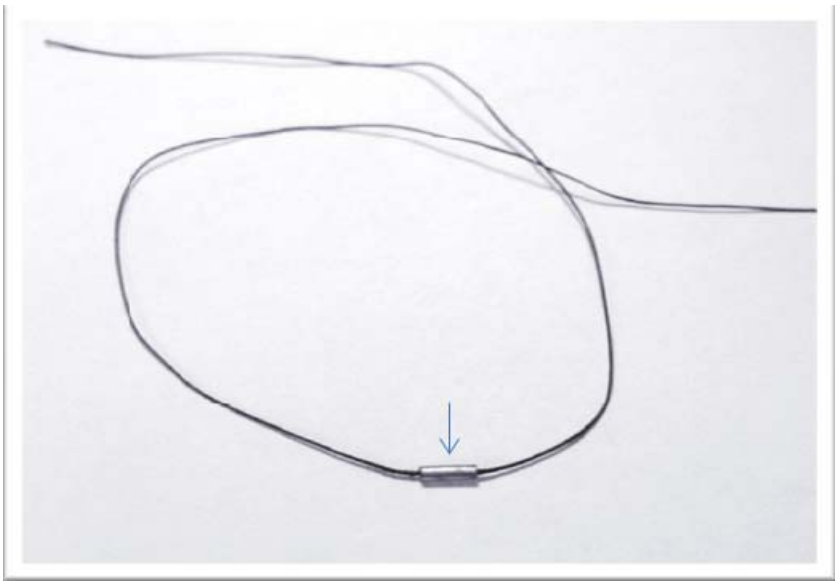

Figure 10. Luer stub adapter. A 16G luer stub adapter was used to produce a pulmonary artery (PA) banding of the same diameter in each rat. For practical reasons, the small adapter was thread onto a suture and knot in both ends of the adapter.

To verify the changes in the PA-pressure, right ventricular developed pressure (RVDP) was measured (Formula 2).

$$RVDP = RSP - RDP$$

Formula 2. Definition of right ventricular developed pressure (RVDP). RSP, Right ventricular systolic pressure; RDP, Right ventricular diastolic pressure.

As a PA-catheter is difficult to place in rats, RVDP was measured by placing a 25G i.v. cannula (Terumo Europe N.V., Belgium), into the lumen of the right ventricle (RV) (Figure 11). The cannula was attached to a fluid-filled pressure transducer (Edwards Lifesciences LLC, USA) that was further connected to PowerLab (PowerLab/8SP, ADInstruments Ltd., UK) via an amplifier.

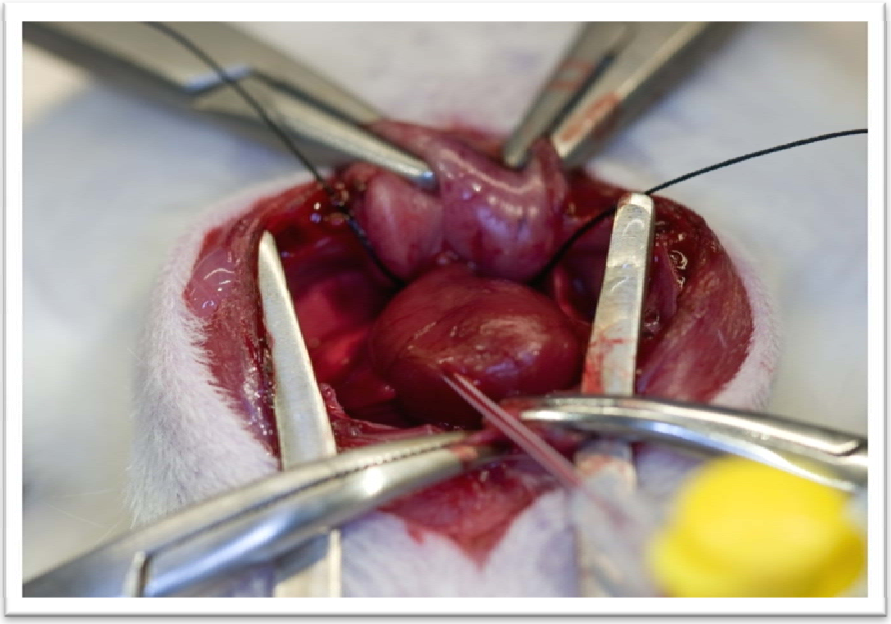

Figure 11. Right ventricular (RV) pressure measurement. The heart was stabilized in a pericardial cradle and a 25G i.v. cannula was placed directly into the RV for pressure measurement.

Depending on protocol, rats undergoing acute procedures were euthanized while still under surgical anaesthesia, whereas rats undergoing chronic procedures were closed thoroughly with suture and allowed to recover. Those animals were treated with post-anaesthetic care, as described in section 2.2.3, to provide good analgesia. Animals were also administrated ~3mL of saline infusion s.c. three times a day during the first two days of recovery, in which animals may not drink within the first 12-24 hours (52). Before ending chronic protocols, rats were re-anesthetized and sternum re-opened to measure RVDP before the heart was excised. Sham operated rats were subjected to the same surgical protocol without PA-banding.

2.3.3 Pressure Measurements and Calibration

PowerLab is a high-performance data acquisition system, capable of recording at speeds up to 200 000 samples per second continuously to disk. Pressure data transferred from the pressure transducer via an amplifier, was converted to mmHg using the software Chart5 for Windows (ADInstruments Ltd., UK). Pressure transducer was filled with physiological saline or ddH_2O, while the pressure catheter (i.v. cannula) was filled with a 20IE/mL Heparin "lock". Air bubbles in the system that could interfere with measurements were avoided. A system calibration was performed before every pressure measurement, keeping the pressure transducer levelled with the heart (Figure 12).

Figure 12. Pressure measurement setup. A fluid filled pressure transducer (A) was connected to a 25G i.v. cannula, used as a pressure catheter (B), placed into the right ventricle of the rat heart for pressure measurement.

A mercury manometer was connected to the pressure transducer and inflated to a level of 200mmHg to calibrate and convert the electric output provided to PowerLab to a level of 200mmHg (Figure 13). The system was thereafter exposed to atmospheric pressure where output was set to 0mmHg (Figure 13).

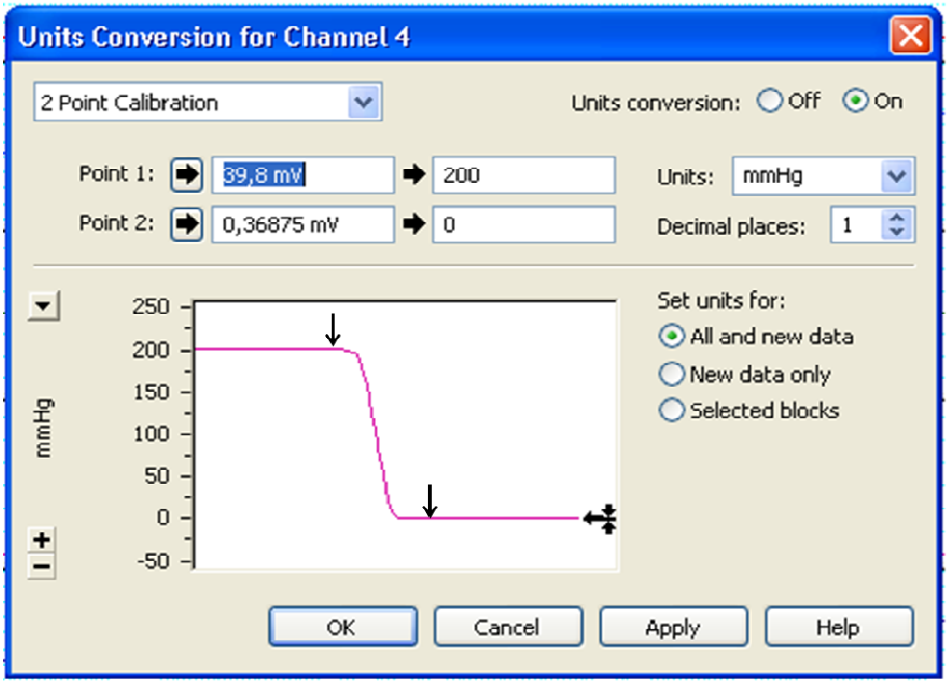

Figure 13. Calibration curve as shown on the computer connected to the PowerLab. A mercury manometer was connected to the pressure transducer and inflated to a level of 200mmHg to convert the electric output (here: 39.8mV) to 200mmHg. The system was then exposed to atmospheric pressure where output (here: 0.36875mV) was set to 0mmHg.

2.3.4 Blood Gases, Hematocrit, Electrolytes and Glucose

To monitor the physiologic condition in the mechanical ventilated rat, sample sizes of ~0.05mL blood was withdrawn directly from the right heart ventricle (RV) via the i.v. cannula placed for pressure measurement. Analyses for blood gas variables (pH, pCO_2, pO_2), hematocrit and various electrolytes (Na^+, K^+, Ca^{2+}, Cl^-) were performed on a blood gas instrument (Radiometer ABL77 Series, Bergman Diagnostika AS, Norway). Derived values, such as haemoglobin, HCO_3^- and sO_2 were also included. Blood glucose was measured utilizing a blood glucose meter (Precision Xceed, MediSense, Abbott Laboratories AS, Norway), using disposable test strips (Precision Xtra Plus, Abbott Norge AS, Norway) requiring only 0.3µL of blood. Calibration of the two instruments was regularly performed.

2.4 Experimental Setup and Treatment Design

Two separate experimental groups were studied at various time points: rats subjected to pulmonary artery (PA) banding and sham rats that were subjected to the same operative procedure, including dissection of the PA, with the sole exception of the placement of the band. Baseline controls (Ctr_{BL}) at time 0 were also included to evaluate the basal level of the total tissue water (TTW) and collagen content. An overview of the experimental setup, including the number (n) of rats is shown in Table 1.

Table 1. An overview of the experimental groups. Number of rats in each group is indicated as n in the parentheses. Ctr_{BL}, Control baseline; Sham, sham experimental groups; PA, pulmonary artery banded experimental groups.

Type of Procedure	Treatment time	Experimental groups	
		Ctr_{BL}/sham (n)	PA (n)
Acute	0 minutes	6	
Acute	30 minutes	6	6
Acute	60 minutes	6	6
Chronic	24 hours	3	2
Chronic	17 days	1	1

During acute experiments (30-/60 minutes of PA-banding), heart function, rectal and thoracal temperatures, glucose and blood gases were regularly monitored as depicted in Figure 14. Heart function variables included right ventricular developed pressure (RVDP), contractility index (dP/dt) and heart rate (HR). RVDP was defined in Formula 2 (section 2.3.2) as the right ventricular systolic pressure subtracted by the right ventricular diastolic pressure. dP/dt (delta pressure divided by delta time), meaning the first derivative of the pressure wave with respect to time, is regarded as an index of the myocardial contractile state, which gives an indication of the rate of rise (dP/dt maximum) and rate of fall (dP/dt minimum) of the right ventricular pressure wave. HR is defined as the number of heart beats per unit time (minutes) (BPM). All monitored variables were reported both pre-PA-banding, i.e. after a pressure measurement stabilization period of 10 minutes, and subsequently post-PA-banding, i.e. after 15- (only heart function variables), 30- and 60 minutes. Chronic experiments (24 hours/17 days of PA-banding) were monitored slightly different, however, in a similar manner (Figure 14). During surgery, when banding the PA, only temperature variables were monitored. At

re-opening, meaning in the end of the chronic protocol, heart function parameters were included in the monitored parameters. After ending experimental protocols, hearts, lungs and biceps femoris muscle were weighed.

ACUTE

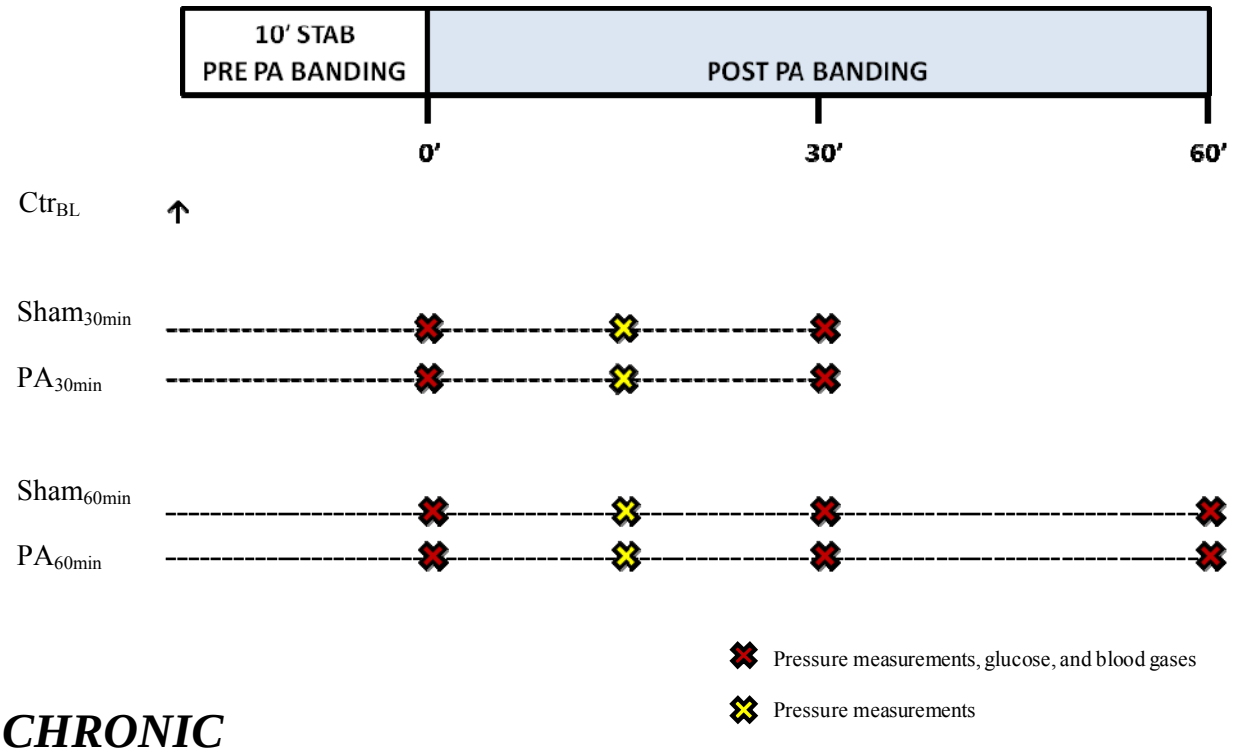

CHRONIC

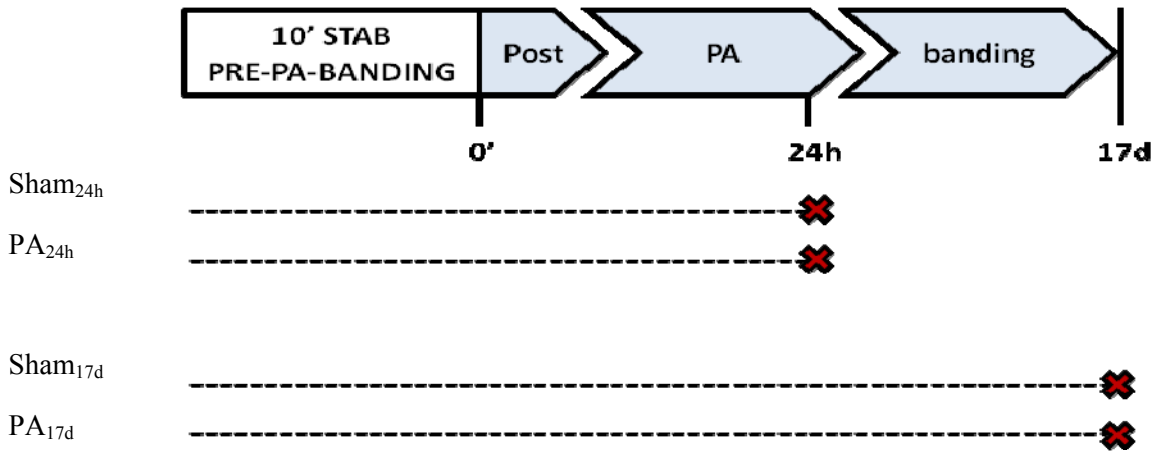

Figure 14. Experimental protocol for acute and chronic procedures. A stabilization period of 10 minutes (10' STAB PRE-PA-BANDING) was allowed before banding the pulmonary artery (PA). Rats were continuously PA-banded from time 0' until end of experiments. Crosses indicate time points at which blood samples were drawn for blood gas- and glucose analyses, in addition to reporting heart function parameters (Right ventricular developed pressure (RVDP), heart rate (HR) and the rate of rise (dP/dt maximum) and relaxation (dP/dt minimum) of the right ventricular pressures). Ctr$_{BL}$, Control baseline; Sham, sham experimental groups; PA, PA banded experimental groups. ', minutes; h, hours; d, days.

2.5 Myocardial Oedema

Total tissue water (TTW) is a measure of the transcapillary water transport resulting in oedema, i.e. the water content in an organ or tissue. TTW content is comprised of vascular water, interstitial water, and cellular water (7). The amount of myocardial oedema or TTW was determined using a gravimetric method, defined as the water content per gram of dry tissue weight [(wet weight – dry weight)/(dry weight)]. To identify the amount of myocardial oedema accumulation, wet to dry ratios were measured at various time points after pulmonary artery (PA) constriction or sham procedures (see section 2.4, Figure 14, for time points). Each heart sample was divided into left and right ventricles and the septum. These were further split into basis, mid and apex. Control samples from the biceps femoris muscle and lungs were subsequently collected. Samples were weighted before drying to obtain wet weight, using a highly accurate scale (Mettler Toledo AX 205 DeltaRange, Mettler-Toledo AS, Norway) set to "fast" user selection with four digit decimals. A blood correction was not performed due to the small sample size. Quantification of myocardial oedema was performed by utilizing a freeze dryer.

2.5.1 Freeze Drying

Freeze drying is a dehydration technique, which enables liquid or slurry products, which have previously been frozen to be dried under a vacuum. Samples were therefore initially frozen to -80°C as soon as possible after sampling, in such way that the product exhibited the desired crystalline structure, and so that it was frozen below its eutectic temperature. Frozen samples were subsequently freeze-dried (VirTis Wizard 2.0 Control System, SP Industries, USA). In order to obtain an end-product of satisfaction, i.e. dry tissue, the partial pressure of the vapour surrounding the product must be lower than the pressure of the vapour from the ice at the same temperature. Additionally, the energy supplied in the form of heat must remain lower than the eutectic temperature of the product (the highest allowable product temperature during the conditions of sublimation). Condenser and vacuum at low temperature (shelf temperature holding at least -20°C) was manually set, during which the sample water sublimated, resulting in a dry tissue. All samples were dried overnight. To control that the tissue samples were sufficiently dry after one overnight freeze drying session, the first sets of samples were subsequently dried another night to confirm that the dry weight was not changed. Vacuum

was thereafter released and the dried tissue was allowed to defrost and stabilize at room temperature for 20 minutes before weighing (Mettler Toledo AX 205 DeltaRange, Mettler-Toledo AS, Norway).

2.6 Collagen Content – Hydroxyproline Analysis

Total collagen was analyzed according to the method described by Woessner (53), based on a hydroxyproline colorimetric assay.

Freeze dried tissue was prepared by hydrolysis without preliminary purification overnight at 120°C, in sealed test tubes in the presence of HCl. Content was allowed to reach room temperature before rinsing and dilution with ddH_2O to a total volume of 4mL. Samples were subsequently diluted with ddH_2O, volume depending on the amount of freeze dried tissue ((225/Xmg freeze dried tissue/4mL)) × 5), to reach a total volume of 4.5mL and a final tissue concentration of 0.25µg/µL.

Experimental reagents and standards were prepared as described in Appendix A. All reagents, except p-dimetylamino benzaldehyde (p-DABA), were stored in a refrigerator, but allowed to reach room temperature before use. p-DABA was solved and stored in a water bath holding 60±1°C. As reactions were time dependant, it was important to keep track of time during the following analytical procedure. Hydrolysed samples were pipetted into soft plastic test tubes, where Chloramine-T reagent was added. Twenty minutes later, Perchloric acid was added, mixed uniformly in the solution, and left at room temperature for 5 minutes, before p-DABA was added. After mixing, the tubes were placed in a water bath keeping 60±1°C, for 20 minutes, before cooled in tap water for 5 minutes to stop the reaction. Sample sizes of 250µL were dispensed in duplicates into microplates with 96 wells (MaxiSorp, NUNC, Denmark). Absorbance was finally read at 557nm using a spectrophotometrical microplate reader (Molecular Devices SpectraMax Plus 384, GMI Inc., USA). Results were displayed through a computer (Pentium processor with Windows XP), using the software Softmax PRO (Molecular Devices, USA).

A standard curve was made that correlated with the amount of hydroxyproline in 125 µg of the sample tissue. Total collagen concentration was correlated to hydroxyproline by a factor of 6.94 (µg collagen/µg hydroxyproline).

2.7 Statistical Analysis

Values were presented as mean ± standard error of the mean (SEM). Body-, heart-, lung-, and skeletal muscle weights, right ventricular developed pressures (RVDP), heart rates (HR), contractility indexes (dP/dt maximum and minimum) of the right ventricular pressures, pH, hematocrit, glucose, and total tissue water (TTW) were tested for group differences by one way analysis of variance (ANOVA) combined with the Fisher post hoc test by using Minitab statistical software (Minitab 15 English.Ink, Minitab Inc., USA). $P<0.05$ was considered statistically significant.

3 Results

The scope of this Master's thesis was threefold. **Firstly**, to establish an *in vivo* model of pulmonary artery (PA) banding, as shown by others (13) to produce myocardial oedema with subsequent fibrosis formation. By reducing the diameter of the PA, the right ventricular developed pressure (RVDP) was expected to increase, giving rise to myocardial oedema, possibly leading to subsequent fibrosis formation over time. Hence, heart function variables, such as RVDP, right ventricular (RV) contractility and rate of relaxation (dP/dt), and heart rate (HR), were monitored to verify the experimental model. **Secondly**, sham- and PA-banded experimental groups were studied to investigate the temporal development of oedema- and fibrosis formation in acute and chronic protocols, respectively undergoing 30-/60 minutes and 24 hours/17 days of banding. **Thirdly**, rat hearts were divided into: (1) RV, left ventricle (LV) and septum, and (2) each further into basis, mid and apex, to investigate a possible spatial distribution of myocardial oedema and fibrosis formation.

Acute protocols were represented by 6 animals in each experimental group, whereas chronic protocols were represented by only 1-3 animals in each group, making statistical data analysis not possible. Chronic procedures were in total performed on 15 rats. Four animals treated with PA-banding died post-operatively, respectively 2-, 3-, 6- and 8 days post surgery, whereas results from three animals (24 hour sham and PA-banded) could not be presented due to an accidental incidence regarding handling of test samples. One sham animal survived however longer than 17 days, but did not fit into any of our experimental protocols, hence, not presented. Consequently, analytical data from 7 rats were left to be presented in the chronic experimental results. An extensive surgical procedure, high mortality rate and an accidental incidence regarding some tissue samples, combined with the restricted time available for this study caused a limited amount of performed experimental protocols and subsequently, a limited representation of the experimental data especially from the chronic protocols.

3.1 Right Ventricular Developed Pressure (RVDP)

Right ventricular developed pressure (RVDP) increased significantly after pulmonary artery (PA) banding in comparison to the initial pressure measured pre-banding (PA_{15min} 43±2mmHg vs. PA_{0min} 23±1mmHg, $p<0.05$) (Figure 15). By contrast, RVDP values in the sham groups did not differ from the initial pressure ($Sham_{15min}$ 29±1mmHg vs. $Sham_{0min}$ 24±1mmHg, ns). Furthermore, RVDP was significantly higher in the PA-banded groups as compared to the sham groups from 15 minutes of PA constriction and throughout experimental protocols (PA_{15min} 43±2mmHg vs. $Sham_{15min}$ 29±1mmHg, $p<0.05$) (Figure 15). However, as chronic protocols were represented by a limited number of animals in the experimental groups, data are only to be considered preliminary. Nevertheless, the preliminary data showed a trend of elevated RVDP in the PA-banded experimental groups as compared to corresponding shams after 24 hours and 17 days (PA_{24h} 41±0.5mmHg and PA_{17d} 35mmHg vs. $Sham_{24h}$ 22±0.3mmHg and $Sham_{17d}$ 17mmHg).

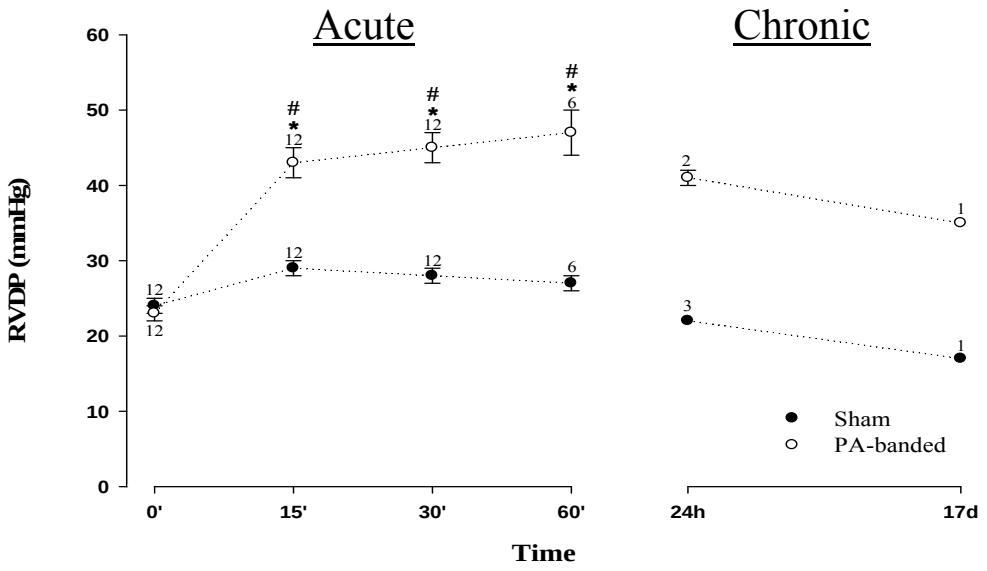

Figure 15. Right ventricular developed pressure (RVDP) during the acute and chronic experimental protocols. All data points from 15 minutes and onwards in the pulmonary artery (PA) banded groups were significantly elevated in comparison to the initial pressure measurement pre-PA-banding (0') and the corresponding sham measurements. Preliminary data show that the RVDP seemed to be elevated still 24 hours and 17 days post-PA-banding as compared to the corresponding sham values. Symbols with error bars represent group means ± SEM. *$p<0.05$ vs. corresponding sham group; #$p<0.05$ vs. initial pressure measured pre-PA-banding (0'). Number of observations is indicated above/under each time point, due to a combined representation of the two experimental groups in the early phase of acute protocols, until sampling 30- and 60 minutes post-banding. However, acute experimental groups were represented by n=6, whereas chronic experimental groups were represented by: $Sham_{24h}$ (n=3); $Sham_{17d}$ (n=1); PA_{24h} (n=2); PA_{17d} (n=1). ', minutes; h, hours; d, days.

3.2 Right Ventricular Contractility and Rate of Relaxation (dP/dt)

Changes in the right ventricular developed pressure (RVDP) during the experimental period were reflected with similar changes in the right ventricular (RV) contractility (dP/dt maximum) and rate of relaxation (dP/dt minimum). dP/dt maximum, i.e. the RV contractility, increased significantly following pulmonary artery (PA) banding in the experimental period (Figure 16). dP/dt minimum, i.e. the RV rate of relaxation, paralleled the changes in contractility with significant decreases (Figure 16).

The PA-banded groups showed a significantly increased contractility (dP/dt maximum) from 15 minutes of banding and onwards, as compared to the initial measurement pre-banding (PA_{15min} 1895±140mmHg/s vs. PA_{0min} 1019±83mmHg/s, $p<0.05$) (Figure 16). Sham values showed, however, no significant changes throughout protocols as compared to the initial measurement ($Sham_{15min}$ 1318±86mmHg/s vs. $Sham_{0min}$ 1078±77mmHg/s, ns). Moreover, the contractility of the PA-banded groups were significantly increased as compared to the corresponding sham values measured 15 minutes post-banding and onwards (PA_{15min} 1895±140mmHg/s vs. $Sham_{15min}$ 1318±86mmHg/s, $p<0.05$) (Figure 16). Contractility reached its maximum at 60 minutes post-PA-banding (PA_{60min} 2708±374mmHg/s), where contractility was significantly and approximately increased by ~115% as compared to the corresponding sham ($Sham_{60min}$ 1261±104mmHg/s) (Figure 16). Preliminary data from the chronic protocols showed that the increased contractility still seemed to be elevated after 17 days of banding in the PA-banded protocol as compared to corresponding sham value (PA_{17d} 1518mmHg/s vs. $Sham_{17d}$ 828mmHg/s) (Figure 16).

From 15 minutes of banding and onwards, the rate of relaxation (dP/dt minimum) was significantly different in the PA-banded groups as compared to the initial value measured pre-PA-banding (PA_{15min} -1427±117mmHg/s vs. PA_{0min} -700±71mmHg/s, $p<0.05$), whereas sham values remained unchanged ($Sham_{15min}$ -1039±65mmHg/s vs. $Sham_{0min}$ -824±61mmHg/s, ns) (Figure 16). The RV rate of relaxation in the PA-banded groups were also significantly different as compared to the corresponding sham values measured from 15 minutes of banding and throughout experimental protocols (PA_{15min} -1427±117mmHg/s vs. $Sham_{15min}$ -1039±65mmHg/s, $p<0.05$) (Figure 16). Preliminary data from chronic protocols showed that the cardiac relaxation seemed to remain changed still after 17 days of banding in the PA-

banded protocol as compared to corresponding sham value (PA_{17d} -1233mmHg/s vs. $Sham_{17d}$ -532mmHg/s) (Figure 16).

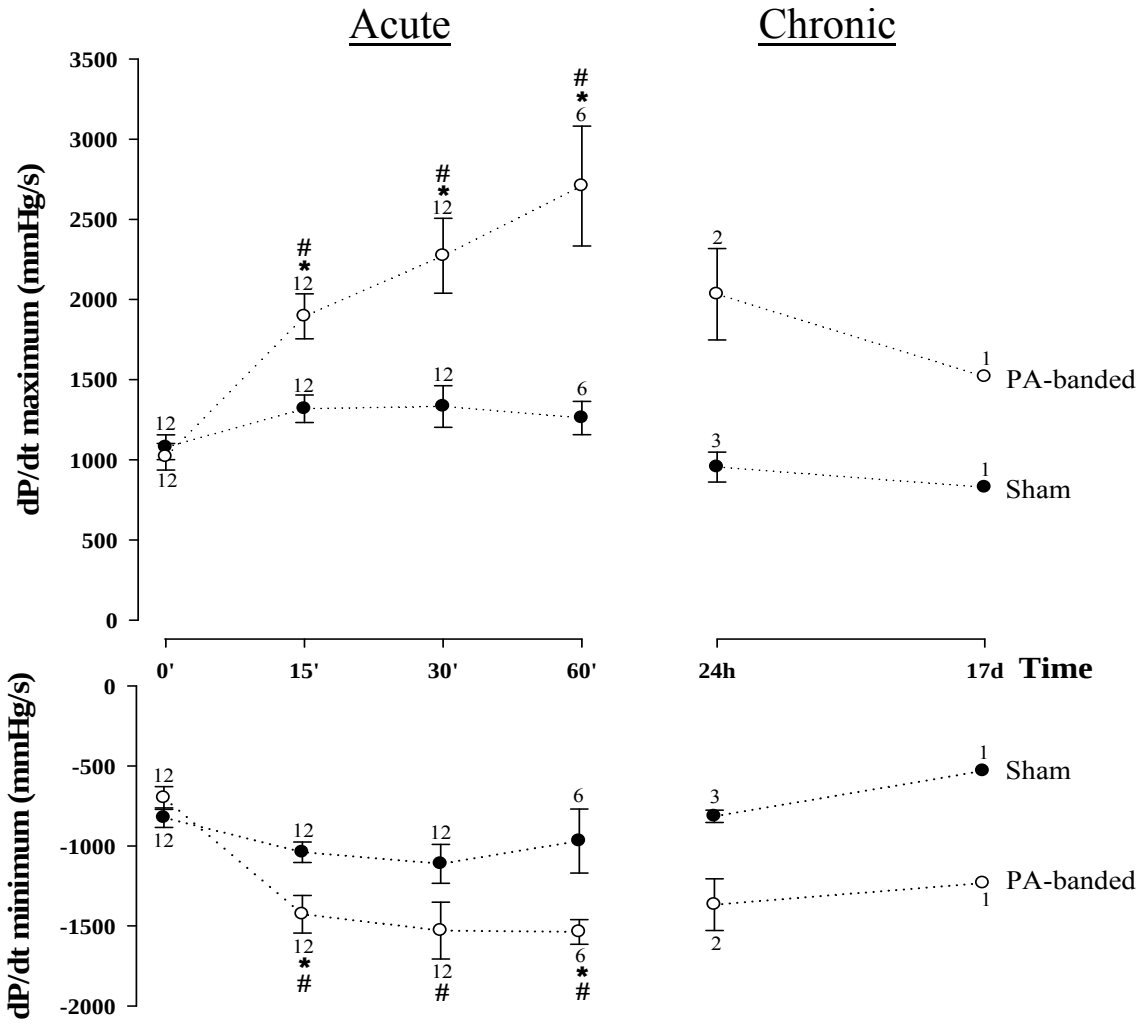

Figure 16. Right ventricular (RV) contractility and relaxation calculated as the first derivative of the right ventricular pressure wave (dP/dt). The pulmonary artery (PA) banded groups showed significantly increased contractility (dP/dt maximum) from 15 minutes and onwards, as compared to the initial measurement pre-PA-banding and the corresponding measurements in the sham groups. Similarly, the rate of relaxation (dP/dt minimum) was significantly different in the PA-banded groups from 15 minutes of banding as compared to the initial value of the same group, and as compared to the corresponding sham values. Symbols with error bars represent group means ± SEM. *$p<0.05$ vs. corresponding sham group; #$p<0.05$ vs. initial pressure measured pre-PA-banding (0'). Number of observations is indicated above/under each time point, due to a combined representation of the two experimental groups in the early phase of acute protocols, until sampling 30- and 60 minutes post-banding. However, acute experimental groups were represented by n=6, whereas chronic experimental groups were represented by: $Sham_{24h}$ (n=3); $Sham_{17d}$ (n=1); PA_{24h} (n=2); PA_{17d} (n=1). ', minutes; h, hours; d, days.

3.3 Heart Rate

The heart rate (HR) of the pulmonary artery (PA) banded groups of the acute protocols were not represented by significance until 60 minutes post-banding as compared to the corresponding shams (PA_{60min} 425±13 beats per minute (beats/min) vs. $Sham_{60min}$ 377±17 beats/min, $p<0.05$) (Figure 17). However, no difference was seen between the PA-banded value and the initial measured value pre-PA-banding after 60 minutes (PA_{60min} 425±13 beats/min vs. PA_{0min} 369±21 beats/min, ns) (Figure 17). Preliminary data from the chronic protocols indicated a tendency of a collective and relative HR increase of about ~10-15% as compared to the corresponding initial measurements of the acute protocols (Figure 17).

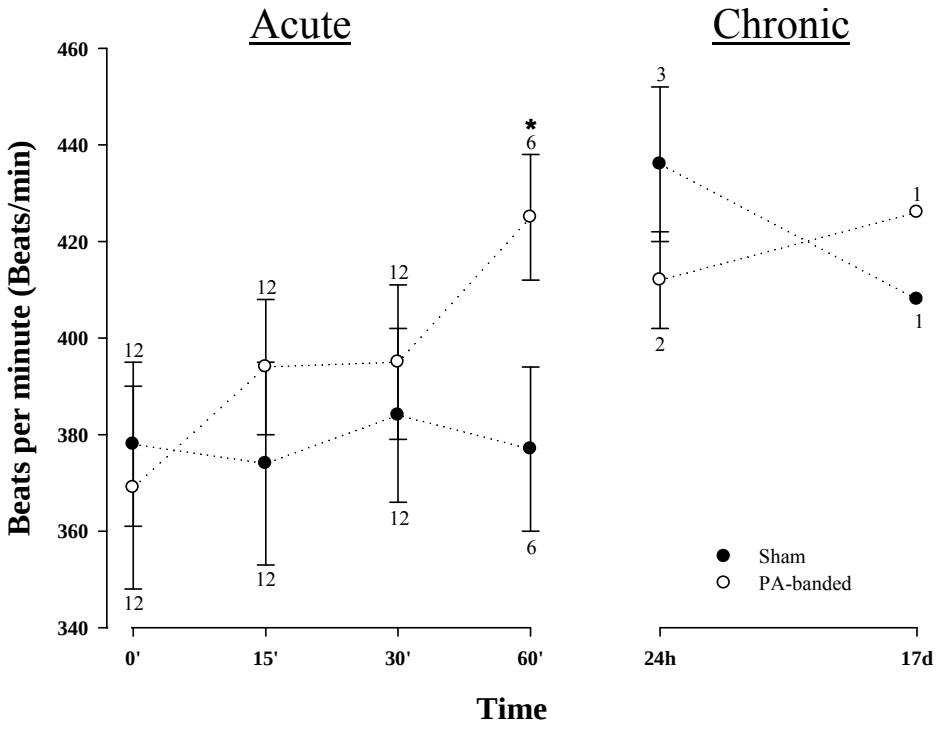

Figure 17. Heart rates (HR) during the acute and chronic experimental protocols. No significant increases in HR were seen until 60 minutes post-banding in the pulmonary artery (PA) banded group as compared to the corresponding sham. However, no significance was seen between the PA-banded value 60 minutes post-banding as compared to the initial measurement pre-PA-banding. Preliminary data from the chronic protocols indicated a tendency of a general HR increase as compared to the corresponding initial measurements of the acute protocols. Symbols with error bars represent group means ± SEM. *$p<0.05$ vs. corresponding sham group. Number of observations is indicated above/under each time point, due to a combined representation of the two experimental groups in the early phase of acute protocols, until sampling 30- and 60 minutes post-banding. However, acute experimental groups were represented by n=6, whereas chronic experimental groups were represented by: $Sham_{24h}$ (n=3); $Sham_{17d}$ (n=1); PA_{24h} (n=2); PA_{17d} (n=1). ‘, minutes; h, hours; d, days.

3.4 Temporal and Spatial Distribution of Oedema in the Heart

In the process of determining the temporal development of myocardial oedema in a pulmonary artery (PA) banded rat model, the spatial distribution of the oedema formation was subsequently investigated. The formation of oedema was determined by a quantitative increase in the amount of total tissue water (TTW) of the myocardial interstitium. Right- and left ventricles and the septum were divided into basis, mid- and apical areas for the investigation of a spatial oedema formation (Figure 18). A baseline control group (i.e. the component concentration level before introducing animals to experimental conditions) was additionally included in the protocols to represent the basal level of the TTW.

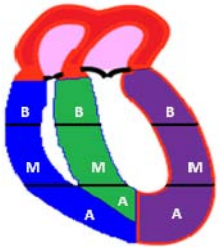

Figure 18. Illustration of the division of the right- and left heart ventricles and septum to determine a possible spatial development of the oedema formation in the heart. Heart ventricles and septum were each separated into basis (B), mid (M) and apical (A) sections.

The main overall features of the TTW explored in the gradient sections of the heart ventricles revealed no differences within PA-banded groups of the acute protocols, i.e. within the first hour of PA-banding, as compared to the baseline control and corresponding shams. In contrast, large increases were seen towards the end of chronic protocols, i.e. after 17 days of PA-banding, as compared to the corresponding shams and values from the acute protocols (Figure 19). Nevertheless, the large TTW changes seen after 17 days are only to be considered as preliminary, due to the limited number of animals in the experimental groups.

No significant changes were seen in the PA-banded groups of the acute phase (30-/60 minutes of PA-banding) as compared to the corresponding shams and respective baseline values (Figure 19). However, the TTW of the left ventricular (LV) spaces showed general trends of reduction as compared to the respective baseline values, with significance only in the sham groups of the LV_{mid} after 60 minutes of banding ($Sham_{60min}$ 3.9±0.1 vs. Ctr_{BL} 4.5±0.2, $p<0.05$) and the LV_{apex} after 30- and 60 minutes of PA-banding ($Sham_{30min}$ 4.0±0.3 and $Sham_{60min}$ 3.8±0.1 vs. Ctr_{BL} 4.5±0.1, $p<0.05$) (Figure 19).

As chronic protocols (24 hours/17 days of PA-banding) were represented by a limited number of animals in the experimental groups, data are only to be considered as preliminary. The 17 day protocols that are represented by one animal in each group are, thus, presented without SEM values. The preliminary data showed that all gradient heart sections of the PA-banded groups experienced a rise in TTW 17 days post-banding, as compared to the corresponding sham- and baseline values (Figure 19). Largest increases were, however, noted in the RV_{basis}, with a relative TTW increase of ~60% as compared to the corresponding baseline value (PA_{17d} 6.8 vs. Ctr_{BL} 4.2±0.2), and a ~70% increase as compared to the corresponding sham (PA_{17d} 6.8 vs. $Sham_{17d}$ 4.0) (Figure 19). $Septum_{apex}$ represented the second highest increase in TTW after 17 days of PA-banding, with a TTW increase of ~30-50% as compared to the corresponding baseline- and sham value (PA_{17d} 5.6 vs. Ctr_{BL} 4.3±0.2 and $Sham_{17d}$ 3.7) (Figure 19).

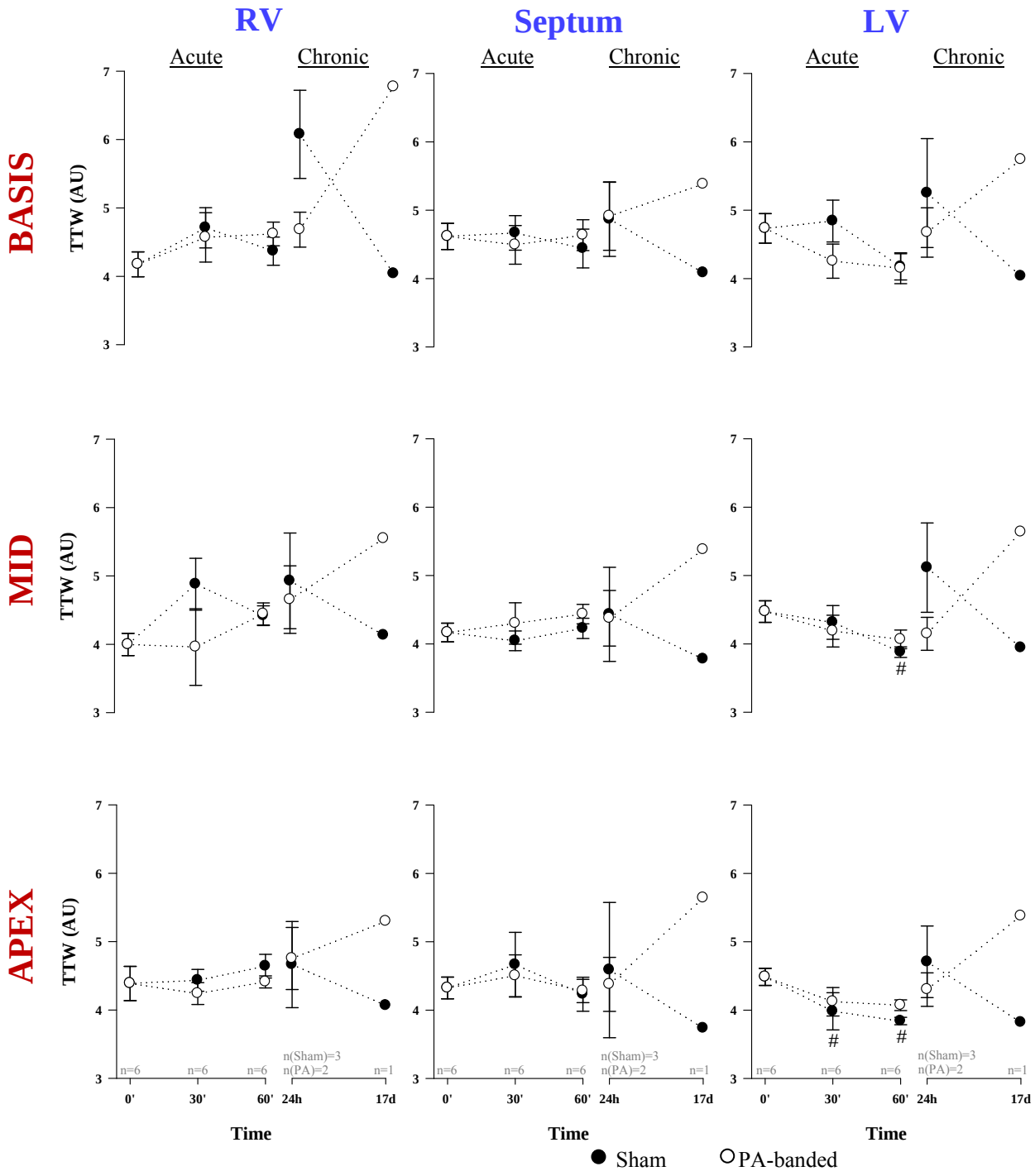

Figure 19. The spatial distribution of the total tissue water (TTW) in the heart. No statistical differences were seen within the acute protocols (30-/60 minutes of PA-banding) in the PA-banded groups as compared to the respective sham- and baseline values. However, a general decreasing trend in the TTW was seen in the left ventricle (LV), only showing statistical difference in the sham values of the LV_{mid} after 60 minutes of PA-banding and the LV_{apex} after 30- and 60 minutes of PA-banding, as compared to the corresponding baseline values. Most pronounced increases in TTW were seen in the preliminary data 17 days post-PA-banding, with the largest increases in the RV basis. Symbols with error bars represent group means ± SEM. #$p<0.05$ vs. initial pressure measured pre-PA-banding (0'). n=6 animals at all measured time points in the acute experimental groups, whereas chronic experimental groups were represented by: $Sham_{24h}$ (n=3); $Sham_{17d}$ (n=1); PA_{24h} (n=2); PA_{17d} (n=1). ', minutes; h, hours; d, days.

3.4.1 Oedema Formation within the Different Ventricles of the Heart

During the process of determining the temporal development of myocardial oedema, the possible spatial distribution (described in section 3.4) of the total tissue water (TTW) of the heart myocardium was additionally explored from another perspective. Basis, mid- and apical sections from the right- and left ventricles and the septum, were summed to represent the respective ventricular TTW within the different experiments (Figure 20). By presenting the data in this way, i.e. by summing the three gradient sections (basis, mid and apex) to give right ventricle (RV), septum or left ventricle (LV), the general picture of the TTW-trends between the heart ventricles were easier to interpret. A baseline control group (i.e. the component concentration level before introducing animals to experimental conditions) was additionally included in the protocols to represent the basal level of the TTW.

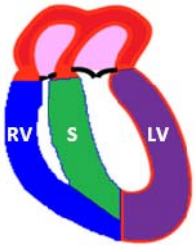

Figure 20. Illustration of the sectioning of the heart as used in the analysis of myocardial oedema. Heart was divided into right ventricle (RV), left ventricle (LV) and septum (S).

The LV pulmonary artery (PA) banded groups of the acute protocols (30-/60 minutes of PA-banding) experienced decreases in TTW after 30- and 60 minutes of banding, as compared to the respective baseline value (PA_{30min} 4.2±0.1 and PA_{60min} 4.1±0.1 vs. Ctr_{BL} 4.6±0.1, $P<0.05$) (Figure 21). No differences were, however, seen in the RV or septum TTW of the PA-banded experimental groups, as compared to the corresponding shams or baseline values.

Focusing on the chronic phase (24 hours/17days of PA-banding), representing, however, only preliminary data, TTW did not seem to have changed after 24 hours, but after 17 days, the TTW was markedly increased in the PA-banded groups as compared to the corresponding baseline values (Figure 21). Largest TTW increases were seen in the PA-banded RV, with a relative increase of ~40% as compared to the baseline- and sham value (PA_{17d} 5.9±0.5 vs. Ctr_{BL} 4.2±0.1 and $Sham_{17d}$ 4.1±0.0), followed by a LV increase with a relative change of ~20-40% (PA_{17d} 5.6±0.1 vs. Ctr_{BL} 4.6±0.1 and $Sham_{17d}$ 3.9±0.1) (Figure 21). Although data from 17 days of chronic protocols were represented by only one animal, figure and statistics were based on the number of samples in each group, hence, giving SEM values for these experiments.

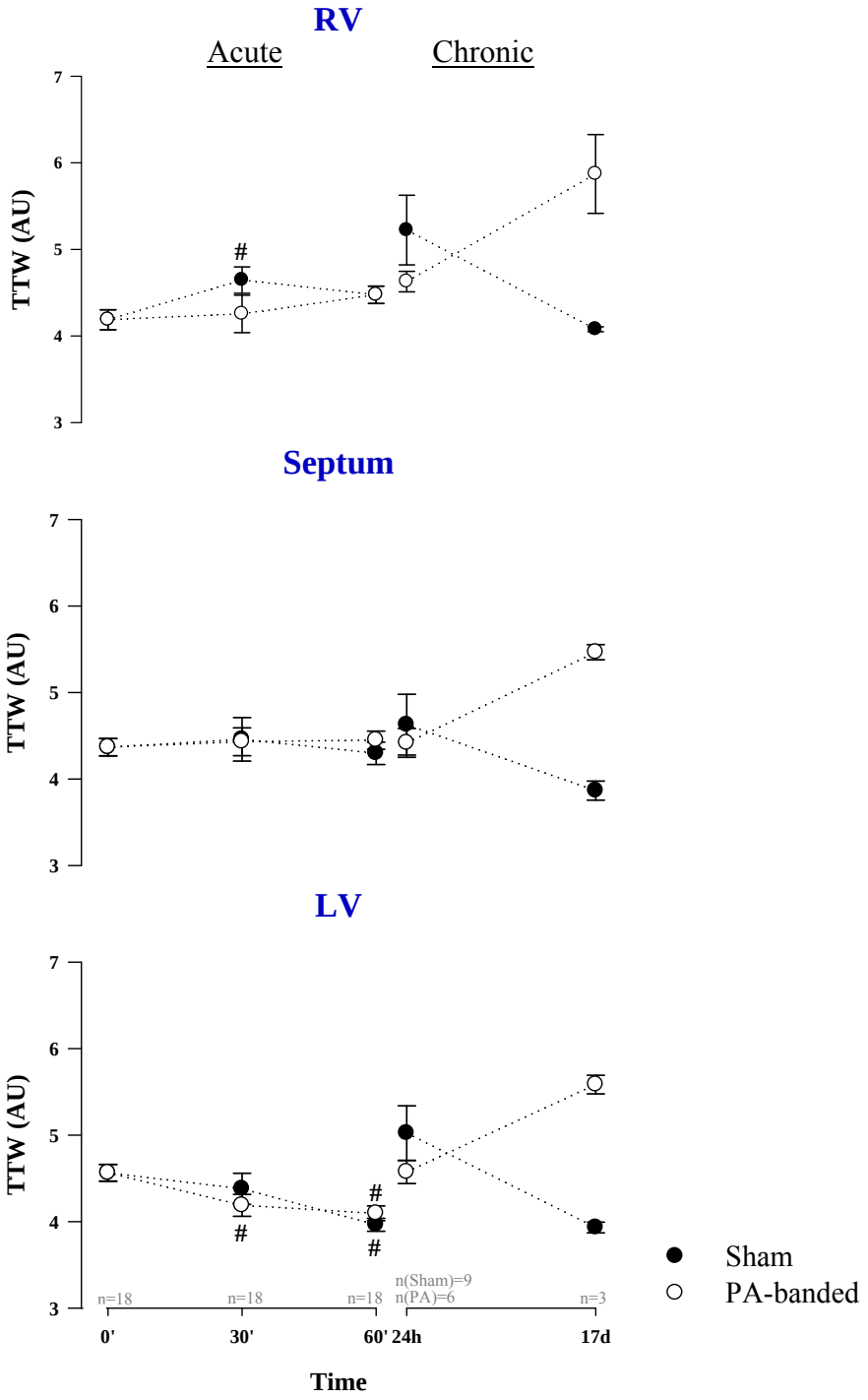

Figure 21. Total tissue water (TTW) of the right- and left ventricles and the septum. Left ventricular (LV) TTW was significantly decreased in the pulmonary artery (PA) banded groups 30- and 60 minutes post-banding. Moreover, a marked, but a non-statistically provable (due to the same origin of the test samples) increase were seen in the PA-banded groups 17 days post-banding as compared to the corresponding shams and baseline values. Symbols with error bars represent the summed test sample means ± SEM. Hence, the one animal representing the 17 day experimental groups are presented with SEM values. #p<0.05 vs. baseline value (0'). n=18 test samples (6 animals) at all measured time points of the acute experimental groups, whereas chronic experimental groups were represented by; $Sham_{24h}$ (n=9; 3 animals), $Sham_{17d}$ (n=3; 1 animal), PA_{24h} (n=6; 1 animal), PA_{17d} (n=3; 1 animal). ', minutes; h, hours; d, days.

3.4.2 Oedema Formation within the Heart

An additional view of the oedema formation in the heart was obtained by exploring it as a whole, i.e. all test samples within the same experiment were summed to represent the TTW of the whole heart, thus yielding nine test samples from one animal. A baseline control group (i.e. the component concentration level before introducing animals to experimental conditions) was included in the protocols to represent the basal level of the total tissue water (TTW).

No differences in TTW were seen in the acute protocol (30-/60 minutes of PA-banding) (Figure 22). Preliminary data from the chronic protocol (24 hours/17 days of PA-banding) demonstrated a marked TTW increase in the experimental pulmonary artery (PA)banded group after 17 days of banding (with the 17 days time point representing nine test samples from one animal, hence presented with a SEM value), showing a relative increase of ~25% as compared to the baseline value (PA_{17d} 5.6±0.2 vs. Ctr_{BL} 4.4±0.1) and ~40% as compared to the corresponding sham (PA_{17d} 5.6±0.2 vs. $Sham_{17d}$ 4.0±0.0) (Figure 22).

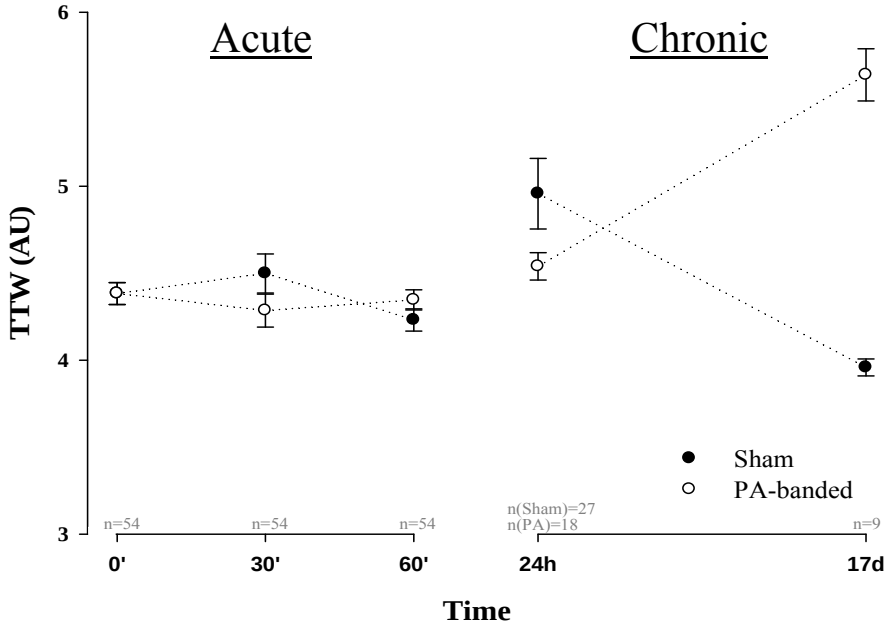

Figure 22. Total tissue water (TTW) of the whole heart. No differences in TTW were seen until 17 days post pulmonary artery (PA) banding, however, represented only by preliminary data. Symbols with error bars represent the added test sample means ± SEM. Hence, the one animal representing the 17 day experimental groups are presented with SEM values. n=54 samples test (6 animals) at all measured time points of the acute experimental groups, whereas chronic experimental groups were represented by; $Sham_{24h}$ (n=27; 3 animals), $Sham_{17d}$ (n=9; 1 animal), PA_{24h} (n=18; 2 animals), PA_{17d} (n=9; 1 animal). ‘, minutes; h, hours; d, days.

3.5 Total Collagen Content in the Heart

Davis et al. (13) has previously demonstrated that myocardial oedema preceded an increased collagen deposition, i.e. fibrosis, and suggested that the oedema played a central role, triggering collagen synthesis and deposition. Along with the investigation of the temporal development of myocardial oedema, subsequent to banding the pulmonary artery (PA) in the *in vivo* rat model, total collagen content was examined to determine the temporal development of fibrosis formation. Due to the limited amount of time available for this Master's thesis, only right ventricular (RV) apical areas were examined. Furthermore, due to a large number of samples, collagen analysis was separated into two series. Experimental results were thereby based on two different sets of standard curves (Appendix A). The first series of samples were, however, not completely hydrolyzed due to insufficient dilution. Thus, these samples might have contained increased amounts of sodium chloride, depressing chromogen formation; resulting in falsely lowered hydroxyproline concentrations and subsequent collagen contents. Baseline controls (i.e. the component concentration level before introducing animals to experimental conditions) were included to represent the basal level of the total collagen content.

No significant changes in collagen content were detected in the acute PA-banded experimental groups as compared to the baseline value (Figure 23). However, a statistical increase was seen after 60 minutes of banding in the sham group as compared to the corresponding PA-banded group ($Sham_{60min}$ 3.2±0.7mg/g dry weight (DW) vs. PA_{60min} 5.0±0.1mg/g DW, $p<0.05$). Moreover, although not statistically proven due to only one animal representing the experimental group, ~140% increase in collagen content was seen after 17 days of banding in the PA-banded experimental group as compared to the control baseline value (Ctr_{BL} 3.5±0.9mg/g DW vs. PA_{17d} 8.4mg/g DW), in addition to ~40% increase as compared to the corresponding sham value ($Sham_{17d}$ 5.9mg/g DW vs. PA_{17d} 8.4mg/g DW) (Figure 23).

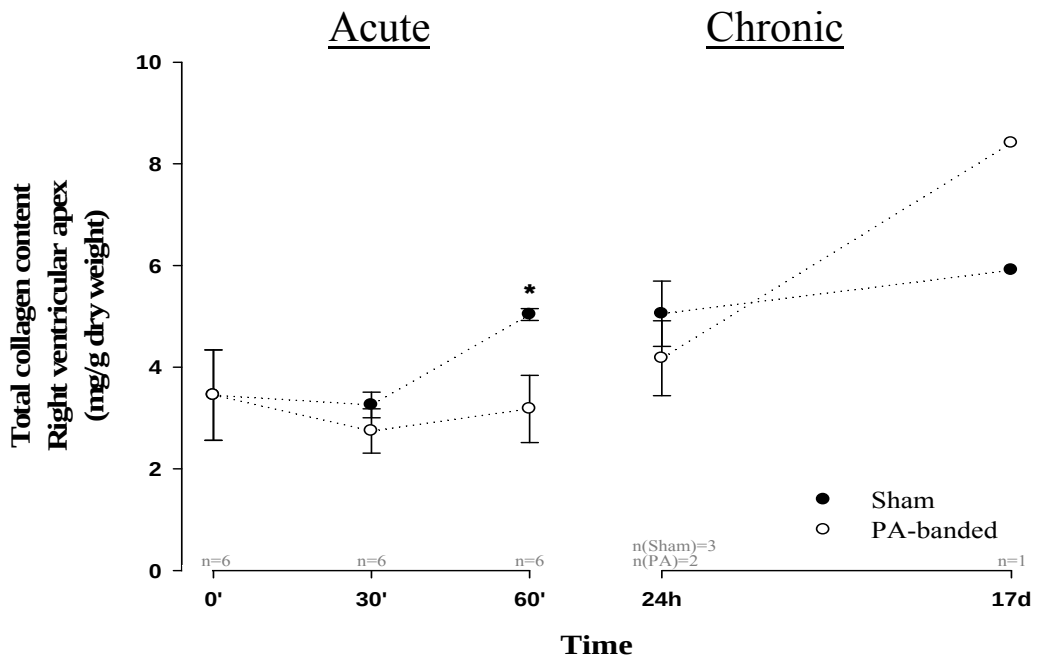

Figure 23. Total collagen content of the right ventricular (RV) apex. No significance was seen in the pulmonary artery (PA) banded groups as compared to the baseline value throughout acute experimental protocols (30-/60 minutes of PA-banding). However, a difference was detected in the sham group 60 minutes post-PA-banding. Preliminary data from the chronic protocols showed a visual increase in the PA-banded group as compared to the corresponding sham and baseline value. *p<0.05 vs. corresponding sham group. n=6 animals in all measured time points except for the experimental groups; $Sham_{24h}$ (n=3), $Sham_{17d}$ (n=1), PA_{24h} (n=2), PA_{17d} (n=1). ‘, minutes; h, hours; d, days.

3.6 Skeletal muscle and Lung Controls

Control samples from skeletal muscle and lungs were included to determine if an eventual increase in total tissue water (TTW) or collagen content was specific to the myocardium, or if the oedema/fibrosis formation was generalized- and/or additionally located to the lungs.

Skeletal muscle analysis showed no statistical variation in TTW or collagen content in the PA-banded groups as compared to the corresponding sham groups or baseline values.

Lung TTW revealed a statistical increase after 60 minutes of banding in both the PA-banded- and the sham group as compared to the baseline value (PA_{60min} 5.7±0.3 and $Sham_{60min}$ 4.9±0.2 vs. Ctr_{BL} 4.4±0.1, $p<0.05$) (Figure 24). Moreover, the PA-banded group was significantly increased as compared to the sham group 60 minutes post-PA banding ($Sham_{60min}$ 4.9±0.2 vs. PA_{60min} 5.7±0.3, $p<0.05$) (Figure 24). However, the TTW increase seen 60 minutes post-banding did not continue into the chronic protocols (24 hours/17 days of PA-banding) (Figure

24). The subsequent analysis of total collagen content in the lungs revealed no differences between the experimental groups.

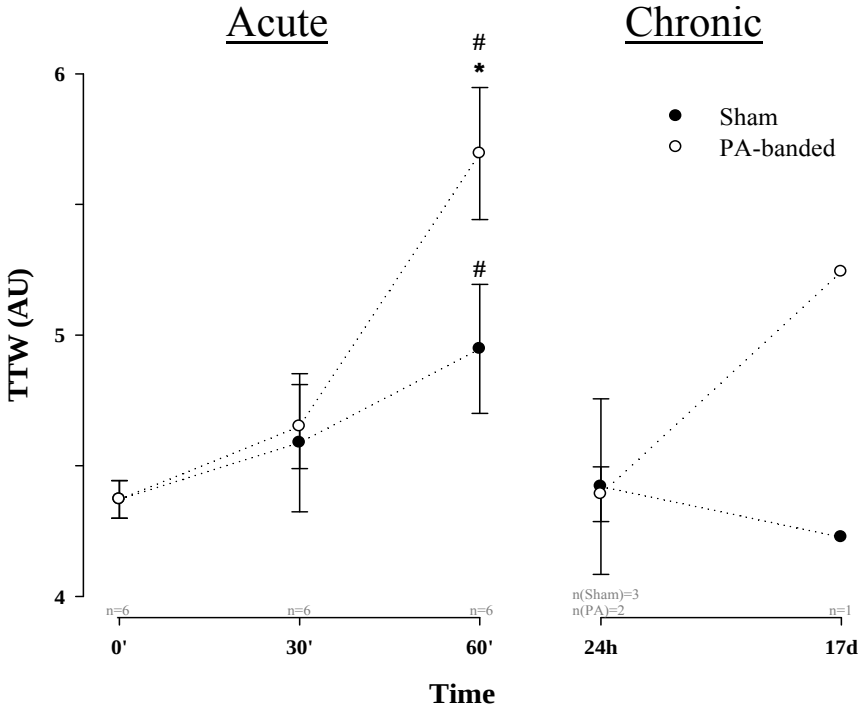

Figure 24. Total tissue water (TTW) of the lung. A general increase in TTW was seen in the lungs during the acute procedures (30-/60 minutes of PA-banding), represented by a statistical increase after 60 minutes of banding in both the PA-banded- and sham group as compared to the baseline value. Moreover, the PA-banded group was significantly increased as compared to the sham group 60 minutes post-PA banding. However, the TTW increase seen 60 minutes post-banding did not pursue into the chronic protocols (24 hours/17 days of PA-banding). Symbols with error bars represent group means ± SEM. *$p<0.05$ vs. corresponding sham group; #$p<0.05$ vs. initial pressure measured pre-PA-banding (0'). n=6 animals at all measured time points in the acute experimental groups, whereas chronic experimental groups were represented by: $Sham_{24h}$ (n=3); $Sham_{17d}$ (n=1); PA_{24h} (n=2); PA_{17d} (n=1). ', minutes; h, hours; d, days.

3.7 General Body- and Tissue Weights

No statistical difference in body weights were seen between the various experimental groups, representing average rat weights prior to surgical procedures of 287±6g for acute- and 349±11g for chronic experimental groups, respectively. Rats undergoing 24 hour chronic procedures had generally lost ~5g of body weight at time of re-opening as compared to before surgical procedures, whereas rats undergoing 17 days of chronic procedures had similarly gained ~5g of body weight.

No variation in heart weights were seen between the experimental groups, except for the one animal undergoing 17 days of PA-banding that showed a weights increase of ~80% as compared to the corresponding sham and baseline heart weights (PA_{17d} 2.26g vs. $Sham_{17d}$ 1.28g and Ctr_{BL} 1.24±0.07g).

No variation was detected in lung- or skeletal muscle weights as PA-banded groups were compared to the corresponding sham groups and baseline value.

4 Discussion

The scope of this Master's thesis was threefold. **Firstly**, in the process of establishing an *in vivo* rat model of pulmonary artery (PA) banding, i.e. by reducing the diameter of the PA, the right ventricular developed pressure (RVDP) was expected to increase, subsequently giving rise to myocardial oedema and increased collagen deposition. Changes in heart function variables, such as RVDP, right ventricular (RV) contractility and rate of relaxation (dP/dt), in addition to heart rate (HR), verified the experimental model. **Secondly**, the goal was to investigate the temporal development of oedema formation and subsequent changes in collagen content. Thus, an acute protocol (30-/60 minutes of PA-banding) and a chronic protocol (24 hours/17 days of PA-banding) were studied to reveal the time points at which changes took place. **Thirdly**, in addition to exploring the temporal development of myocardial oedema and collagen changes, the potential spatial distributional development within the myocardial interstitium was investigated.

Within the time limit available for this Master's thesis, the acute part and immediate post-banding period obtained most of the attention. Nevertheless, the acute experiments demonstrated satisfactory cardiac function. Furthermore, the long term surviving animals demonstrated that this level of banding seemed appropriate for long term experiments.

4.1 Central Findings

4.1.1 Verification of the Pulmonary Artery Banded in vivo Model

Pulmonary artery (PA) banding induces myocardial oedema not only in the right ventricle (RV) where the pressure is increased, but also in the left ventricle (LV), since thebesian veins and sinus venosus together drain the RV and the LV. As LV venous drainage enters the right atrium through the coronary sinus, a RV pressure increase leads to a subsequent coronary sinus pressure elevation, thus increasing LV microvascular exchange vessel pressure and trans-microvascular fluid flux, leading to a left sided oedema. Moreover, as cardiac lymph drains into the central venous system, the pressure elevations leads to a decreased rate of removal of oedema fluid from the LV, further accumulating interstitial water. Since only the

RV experiences pressure overload and a subsequent hypertrophic myocardium, the effects of the LV oedema formation can be studied without interferences from manipulation of the LV itself.

We demonstrated a marked experimental response when permanently reducing the diameter of the PA by banding, in which continuous RVDP elevations of ~50-100% were reported. The permanent reduction of the PA-diameter resulted in a continuous RVDP elevation of ~50-100% in the PA-banded rats throughout the experimental protocols. This relative increase in RV pressure is consistent with other studies, Davis *et al.* reporting a relative increase of 46-144% in RVDP when constricting the PA to the same diameter (against a 16G luer stub adapter) in a similar rat model, and further, ~100% increase in canine models of PA-banding (6, 13).

When increasing the RVDP by PA-banding, we postulated that an immediate compensation would take place, lasting as long as the heart would be able to overcome the increased pressure. We expected to see a steady increase in the heart rate (HR) paralleled with a decrease in the contractility performance and rate of relaxation (dP/dt) as the myocardial oedema would progress. The background for this was that, since oedema is associated with increased chamber stiffness, the quality of each contraction and subsequent relaxation (dP/dt) would deteriorate, resulting in a larger compensation through a increased HR. A study performed in dogs by Laine (35), analyzing the contractility in the LV after occluding the coronary sinus pressure, supported the hypothesis of a decreased dP/dt as oedema progressed. Their experimental records showed an immediate increase in dP/dt maximum, lasting only shortly though, before a steady decrease was seen as oedema evolved. Although our study measured dP/dt in the RV, similar results as Laine (35) were expected. From the time of PA-banding and onwards, we experienced significantly improved contractility performances with subsequent relaxation, while HR remained unchanged in the larger part of the experimental procedures. Urashima *et al.*(54) support this finding, reporting an immediate dP/dt increase post-banding in a murine model of PA-banding. Within the time frame available for this Master's thesis, especially chronic protocols were represented with a limited amount of experimental data. With only one PA-banded rat surviving 17 days of PA-banding, only preliminary conclusions of the results should be made. Nevertheless, the preliminary data still showed an improved dP/dt, indicating that the heart was still trying to compensate for the increases in RV pressure through an increased contraction, followed by better relaxation.

4.1.2 Temporal Development of Myocardial Oedema and Fibrosis

By determining the temporal development of myocardial oedema and subsequent fibrosis formation in an established pulmonary artery (PA) banded model, this model could be used in the specific process of revealing an effective treatment method for oedema- and fibrosis associated diseases. Furthermore, verifying the exact timeframe for oedema- and fibrosis development could reveal the optimal time point for administration of prophylactic interventional treatments. Nedrebø *et al.* (55) has previously shown insulin to prevent a lowering of the interstitial fluid pressure (P_i) during inflammation in the rat skin, attenuating oedema formation after an intravenous treatment of pro-inflammatory cytokines (lipopolysaccharide (LPS), tumor necrosis factor-α (TNF-α) and interleukin-1β) that are known to be produced by many cells during acute and chronic inflammation. The potential anti-inflammatory and anti-oedematous effects of insulin should thus, also be investigated in the heart (section 4.3).

Our results were based on both acute- and chronic protocols, with rats undergoing 30-/60 minutes and 24 hours/17 days of PA-banding, respectively. Data were explored in three different ways to view the results from different spatial aspects. By doing so, both overall- and more specific regional changes were easier to detect. Nevertheless, the analyses revealed similar overall temporal trends. Total tissue water (TTW) did not significantly increase within the first hour after PA-banding, indicating that oedema is not developing within this timeframe. These results also indicate that the Starling forces are still kept within steady state and that the three consecutive lines of defence described by Aukland (28), i.e. the local factors regulating the interstitial fluid volume, are still compensating for the increased RV pressure. Due to a limited number of animals in the chronic experimental protocols, results should be considered as preliminary indications. The preliminary results from chronic protocols showed the expected trend of oedema formation in the PA-banded groups after 17 days of experimental banding. However, after 24 hours of banding, we experienced opposite trends, with TTW elevations in the sham higher than the PA-banded experimental group. The mechanism behind this occurrence is unknown, and may be incidental and possibly altered when increasing the number of animals in the experimental groups.

Myocardial oedema was expected to have developed within 24 hours, as previously shown by others, e.g. Davis *et al*. (13) who demonstrated a marked increase in TTW after 24 hours of PA-banding, utilizing the same experimental rat model as us, i.e. the study was performed in

male rats within a similar weights range, in addition to reducing the diameter of the PA similarly to yield a PA-thickness of 1.52 mm (by tightening the PA against a 16G luer stub adapter). Additionally, their permanent reduction in PA-diameter resulted in an RVDP elevation of 46-144% (13), similarly to us, reporting continuous RVDP elevations of ~50-100% post-PA-banding. The only difference regarding RV pressures were the initial starting points, with Davis *et al.* (13) reporting pressure-means of 9-13mmHg as compared to our 23-24±1mmHg. If the ~10mmHg pressure difference is due to the measuring technique or equipment may only be speculative. As will be mentioned in section 4.2.3, we examined different cannula-sizes to find the smallest one providing us with least chance of bleeding and damage to the rat myocardium, but yet steady signals, and found this to be the 25G cannula. Testing the smaller 27G needle as used by Davis and co-workers, it did not provide us with any reliable pressure signal. Nevertheless, as long as the relative pressure increases were withheld, the initial starting pressure would be expected to have minor consequences on the results. The eventual discussion may, however, be focused towards methodological aspects of the weighing and drying of the sample tissues. Davis *et al.* (13) dried the tissue until constant weight, in comparison to freeze drying the samples overnight as done in our study. As will be described (section 4.2.4), possible variations within the two methodological methods should be investigated. It is also important to note that the differences in TTW are rather small and may easily be overlooked without careful quantification. Optimizing quantification- and analysis techniques would be particularly important in the search for the temporal progression of TTW from normal limits to oedema.

Myocardial interstitial fibrosis is a common manifestation in response to the presence of myocardial oedema, and is known to compromise cardiac function (7, 13, 43, 56). Thus, as no myocardial oedema seemed to be developed within the first hour of PA-banding, neither collagen content was expected to be raised. Results from the collagen analysis of the RV apex were consistent with these expectations. Davis *et al.* (13) reported elevated TTW and oedema formation after 24 hours of PA-banding, preceded by an increased collagen synthesis after 7 days. As the collagen content was not increased after 3 days, i.e. the first measured time point after 24 hours, but after 7 days of PA-banding, this demonstrated that the increased collagen synthesis took place between 3-7 days post-PA-banding (13). As our preliminary data indicated that an oedema was present 17 days post-PA-banding, total collagen content might also be expected to be increased by this time. Subsequent collagen analysis of the RV apex revealed that collagen content seemed to be increased. The level of total collagen

content was, however, in general about 10-fold lower than that of other reported levels of total collagen content in the myocardium (7, 13). Davis *et al.* (13) reported RV baseline values of 27±0.46mg collagen/g dry weight (DW) as compared to our level of 3.5±0.89mg collagen/g DW in the RV apex. This difference may well be related to the insufficient dilution during the first analytic series. Even when dilution was correctly performed, the present values were well below those of Davis *et al.* (13). Hence, it will require follow-up studies to clarify this discrepancy. Nevertheless, Davis and co-workers reported a 3.7-fold increase in total collagen content 28 days after PA-banding, which correlated well with the 2.4-fold increase that we demonstrated in our study (13).

4.1.3 Spatial Development of Myocardial Oedema and Fibrosis

Acute experimental protocols (30-/60 minutes of PA-banding) demonstrated that myocardial oedema was not developed within the first hour of PA-banding in our *in vivo* rat model. Preliminary results from chronic protocols (24 hours/17 days of PA-banding) indicated, however, presence of oedema 17 days post-PA-banding, although based on only one experiment, with large increases in the total tissue water (TTW) located to all the investigated tissue regions. However, the largest relative TTW increase was seen in the right ventricle (RV), and within the RV, the basis sectioned TTW was elevated the most. Further investigations of the time points around the developing phase of myocardial oedema would be essential in the process of revealing exact spatial distributions of the TTW in oedema situations, in which the individual TTW increases and progressions to give oedema would be easier to reveal. Water content in the different regions of the oedematous heart myocardium has previously been elucidated in the domestic swine by Jia *et al.* (57), provoking oedema by hemodilution. Gradient TTW differences were demonstrated within the ventricles and septum, with the largest amounts reported in the RV free wall, followed by septum and the left ventricle (LV) (57). It was suggested that the mechanism behind the findings of higher TTW indexes in the RV and septum could be related to their lower myocardial tissue pressures, diminished vascularity, and lower blood flow as compared to the LV (57). One could also speculate if the RV becomes oedematous because of the thin-walled structure, that the strong mechanical activity of the LV enhances lymph flow, thus reducing the oedema development. Our preliminary finding of the largest amount of TTW in the RV is, thus, so far working in concordance with literature (57). Inter-ventricular TTW differences have also

been observed by others (9, 13). Pratt *et al.* (9) observed in a canine model of coronary sinus hypertension that the RV and LV TTW was increased, whereas the septum TTW remained unchanged. Moreover, Davis *et al.* (13), investigating only the right- and left ventricular TTW in a PA-banded rat model, noted increases in both ventricles, however, with a larger TTW increase in the RV than the LV. Jia and co-workers elucidated additionally to the gradient differences within the heart ventricles and the septum, also internal TTW differences within the LV free wall (57). TTW seemed to accumulate to a higher extent in the apical areas of the LV, followed by mid sections and the basis (57).

As the collagen content was only analyzed within the right ventricular apex, no spatial distributional findings and subsequent interpretations was possible. However, as myocardial interstitial fibrosis supposedly is a manifestation in response to the presence of myocardial oedema, fibrosis would be assumed to be related to the amount and regional locations of the oedema.

4.2 Methodological Aspects

4.2.1 Animals

Experimental procedures were performed on male Wistar rats. Rats are among the most commonly used animals in experimental work, as they are easily bred and handled; in addition that housing can be limited to a relatively confined area. This is not only important for practical reasons, but also economical. Subsequently, the anatomy, physiology, genetics and behaviour is well elucidated, giving results that, if interpreted with consideration, to some extent can be extrapolated to humans.

Optimizing handling- and surgical technique were main focuses during preparations in order to minimize stress in animals throughout the experimental procedures. This was due to the fact that stress is highly associated with increased physiological and biochemical results variability.

4.2.2 Anaesthesia

Animals were subjected to the following anaesthetic regime to provide minimum stress and pain throughout the experimental procedures:

1. Pre-anaesthetic care: Hypnorm (Fentanyl citrate and Fluanisone) or Mebumal (pentobarbital)
2. Peri-anaesthetic care: PropoVet (propofol)
3. Post-anaesthetic care: EMLA cream (lidocain and prilocain) and Temgesic

Animals were treated with pre-anaesthetic care in order to provide a stress-free induction phase for the animals during the intravenous (i.v.) cannulation of the tail vein. Brammer *et al.* (50) previously described Hypnorm to produce heavy sedation, in addition to work well in combination with propofol. With this in mind, Hypnorm was chosen as pre-medication. We experienced an unfortunate and sudden delivery stop from the manufacturer in the middle of surgical experiments, so that Hypnorm was temporarily unavailable. Hypnorm was consequently substituted with Mebumal, a commonly used anaesthetic in circulatory research, having few circulatory side effects. Being a barbiturate and not an analgesic, we experienced calm animals prior to the i.v. cannulation, but a slightly larger reaction response during insertion of the cannula. However, animals seemed to respond quickly to the subsequent i.v. bolus injection of PropoVet, resulting in deep anaesthesia. Furthermore, by changing the pre-anaesthetic regime from Hypnorm to Mebumal, hemodynamic parameters did not seem change, thus indicating no effects between the two.

Brammer and colleagues has previously shown in a study comparing various injectable anaesthetic agents and combinations, that propofol, with Hypnorm pre-medication provided stress-free induction, easily controlled anaesthesia, good analgesia and muscle relaxant for surgery, up to 3 hours duration (50). Moreover, stable and normal heart rates (HR), blood pressures and respiration rates were reported (50). By obeying the recommendations of keeping a continuous infusion of 4-6mL/kg/h propofol to maintain deep anaesthesia subsequent to pre-medication and a propofol bolus dose, we experienced deeply anesthetized rats (50). However, cardio-depression and death were frequently experienced, particularly in many of our acute procedures as these surgical protocols lasted longer than the chronic procedures. By reducing the PropoVet dosage to a minimum, nevertheless, still providing adequate- and deeply anaesthetized rats, cardio-depression was no longer experienced, which indicates a possible concentration dependency of propofol. Indeed, this has previously been

suggested, e.g. Hamilton *et al.* showed in their study that propofol produced a concentration-dependant reduction in evoked contraction at concentrations greater than 5μM, with maximum effect observed at >100μM (58). Various mechanisms for this propofol-induced inotropy have been suggested, e.g. (1) K^+ channel mediation, when studied in atrial muscle (59) and (2) Ca^{2+} uptake capacity impairment of the sarcoplasmatic reticulum in cardiomyocytes (60). However, a study performed by Riou and co-workers (61) *in vitro* to avoid impact from changes in preload, systemic resistance, baroreflex activity, and central nervous system activity, showed only moderate changes on the intrinsic myocardial contractility, suggesting that cardiovascular depression seen with propofol *in vivo* was not related to an intrinsic myocardial depression. Whether propofol contributes to a direct negative inotropic effect is obviously controversial, even though most authors agree that it induces cardiovascular depression. However, propofol should not only be associated with adverse effects, in which one great advantage was the rapid recovery time after disconnecting anaesthesia after the surgical procedure in the chronic protocols. An additional advantage of regaining consciousness quickly after surgery, was the opposed risk of serious hypothermia in the animals. Anaesthesia and surgery commonly cause hypothermia, resulting from a combination of a cool (colder than body temperature, 37°C) operating room and an anaesthetic-induced impairment of the thermoregulatory control (62). Hypothermic animals will have a decreased metabolism and circulation, which, in addition to influencing the experimental results, will prolong recovery time after surgery. To avoid heat loss and hypothermia, the anesthetized animals were placed onto a temperature controlled operation tablet. Regular control of both rectal and thorax (under surgery) temperatures assured optimal temperature conditions for the animals during surgery and post-surgically, until normal thermoregulatory mechanisms were recovered.

4.2.3 Surgical Procedure – Considering Possible Sources of Errors

The heart and pulmonary artery (PA) was accessed via median sternotomy, a normal, but extensive procedure in cardiothoracic surgery. The pericardium is a thin, fibrous, bag-like structure within which the heart lays, only separated by a small amount of lubricating fluid to allow smooth movement of the heart during contraction and relaxation, without disturbances of the surrounding lungs. To reach the PA, the pericardium was opened. Leaving the pericardium open after cardiothoracic surgery is a routine practise in man, hence, being one reason for doing so also when closing the animals after surgery in the chronic protocols. In addition, being a thin and delicate membrane, the rat pericardium would be difficult to close. Moreover, hemodynamic performance is said to be generally better when the pericardium is left open, in addition to reducing the risk of cardiac tamponade (63).

The PA-banded procedure was performed by dissecting the PA from the surrounding tissue, mainly aorta, followed by passing and tightening a silk suture around to elevate the ventricular pressure. Cardiac function and fluid balance may not, however, only have been influenced by the PA-constriction itself, but also by the extensive surgical intervention and the short occlusion during PA-banding, when tightening the suture against the luer stub adapter. However, by including sham controls that are regarded as placebo controls in experimental procedures, and the most rigorous comparator by which to assess the efficacy of an intervention, this possible source of interference was considered.

Right ventricular developed pressure (RVDP) was measured in order to verify changes in the PA-pressure pre- and post-PA-banding. As a PA-catheter is difficult to place in rats, RVDP was measured by placing a 25G i.v. cannula directly into the lumen of the right ventricle (RV). This is an invasive procedure that possibly could interfere with hemodynamics and cardiac physiology, in which the cannula perforated the RV myocardial tissue later sampled for oedema- and fibrotic analyses. Optimally, to reduce the impacts on the experimental results from these measurements, pressure and HR signals from various sized cannulas and syringes were tested in advance, in order to find the smallest functional cannula giving least perforation through the RV. The 25G cannula was the smallest one giving satisfying and steady signals, thus used in the experiments. As previously stated, sham controls were important in the process of revealing these possible additional interferences. The i.v. cannula was attached to a fluid-filled catheter, further connected to PowerLab for hemodynamic pressure- and heart rate (HR) measurements. Hence, PowerLab measures the transferred

pressure- and rate of the fluid filled in the catheter and not directly on the actual blood. Air trapped in the system was avoided and always checked prior to measurements, as pressure transferred via intermediate air bubbles consequently would result in a dampening of the signal. The PowerLab was calibrated prior to every experiment to assure optimal measurements, since systemic drifting could be expected from time to time.

Adult rats have a blood volume of approximately 70mL/kg, giving a total of 14mL of blood in a 200g weighed rat (52). 10% of this volume may be withdrawn at once without particular side effects, whereas a larger removal (>20-25%) will produce signs of hypovolemia, in addition to being a supplemental source of variable and inconsistent experimental results (52). To keep track of blood status, haemoglobin and hematocrit-levels were regularly monitored when blood was sampled. Blood samples were also taken to monitor blood gases and glucose levels. Samples were drawn from the RV, containing venous and oxygen-poor blood. Blood gases are, however, optimally sampled arterially for lung status, but in our case, to obtain an approximate status of the artificial ventilation, venous blood was regarded as sufficient. Glucose analysis was included to monitor the glycemic status, i.e. to assure that none of the rats were hypo- or hyperglycaemic. After sampling, and also throughout the surgical protocol, blood volume was replenished by regularly infusing saline, in order to prevent hypovolemia in the animals. Excessive hypovolemia may occur post-operatively, in which animals may not drink within the first 12-24 hours (52). Thus, animals undergoing chronic procedures were administrated three times a day with ~3mL of saline infusion s.c. during recovery the first two days post surgery, due to the approximate requirements of 40-80mL/kg/24 hours for most animals (52).

4.2.4 Myocardial Oedema – Method Evaluation

Determination of total tissue water (TTW) and oedema formation was performed by freeze-drying the samples (section 2.5). Another, and perhaps more commonly used and well established method in research is the drying chamber, drying tissue in a temperature of ~50°C until constant weight. The offset for not utilizing this method was the limited possibilities for using the tissue subsequently. In which overnight freeze-drying not only is time-saving, but also tissue-preserving, it could have been interesting to investigate possible results-differences between the two methods.

4.2.5 Collagen Content – Hydroxyproline Analysis

Total collagen content was analyzed according to the method described by Woessner (53), based on a hydroxyproline colorimetric assay. Hydroxyproline is widely used as a co-determining indicator of collagen content. This analytical assay is manual and stepwise, additionally to being highly depending on precision and accuracy regarding volumes, reaction times- and temperatures, and is thus, associated with several pitfalls. The method is generally well established in our lab, so that volumes, concentrations and temperatures were already optimized. However, neither heart nor lung samples had previously been analyzed before in our group. The hydroxyproline assay as described by Woessner (53), included two different protocols depending on the amount of hydroxyproline expected to be found in the respective tissue (Method I: for samples containing >2% hydroxyproline; Method II: for samples containing <2% hydroxyproline). Based on hydroxyproline content normally found within the myocardium and lungs, method I was used. However, as heart and lungs were analyzed for the first time in our laboratory, and as for other tissue, the protocol should have been optimized for these tissues. Further follow-up and fine tuning in our laboratory will be required before this is a routine analysis for collagen in heart and lungs.

4.3 Future Perspectives

The present study opens for many further studies. First of all, the number of animals in the chronic experimental groups needs to be increased in order to conclude on the oedemic- and fibrotic responses in the *in vivo* experimental model of pulmonary artery (PA) banding. It would also be necessary to conduct more experiments, investigating the process of the temporal and potential spatial distribution of myocardial oedema and fibrosis development. Expanding acute protocols to 3- and 6 hours would be essential in the further process of investigation, because increased TTW, i.e. myocardial oedema, has previously been demonstrated after 3 hours of coronary sinus pressure elevations in a canine model (7), indicating that this also could be the case for rats. Even though we did not even demonstrate oedema formation after 24 hours of PA-banding, increasing the number of animals in the experimental group could yield other findings. Moreover, expanding chronic protocols to include also 5-, 7- and 12 days of PA-banding would be essential in the process of determining the temporal and potential spatial distribution of a collagen content increase and fibrosis formation.

Further, gene-regulations and histology markers should be included in future studies, as well as determination of the ability of matrix metalloproteinases (MMPs) breaking down collagen, as a process of investigating the oedema development and subsequent collagen deposition. Computerized morphometry on Sirius-red stained tissue sections, in addition to investigating other markers of fibrosis, e.g. by Western blotting, confocal and fluorescent microscopy, or electron microscopy (EM) should be included.

Temporal development of both myocardial oedema and fibrosis would be important to elucidate in an established PA-banded experimental model, also with a clinical application in mind. Insulin therapy has previously been shown by Nedrebø *et al.* (55) to prevent a lowering of the interstitial pressure (P_i) during inflammation in the rat skin, attenuating oedema formation. The potential anti-inflammatory and anti-oedematous effects of insulin should, thus, also be investigated in the heart. Hence, in order to find the most effective time for therapeutic treatment, in addition to answering how optimal administration should be carried out, the temporal time for oedema- and fibrosis formation should be investigated.

Appendix A

Determination of Hydroxyproline

The starting material for this analysis is freeze dried samples.

1. Hydrolysis

a. Fat free freeze dried samples are finely chopped on a small, smooth paper piece using a scalpel (alternatively use a homogenisator). The chopped samples are weighed (set to "home" and registered with 5 decimals).

b. Transfer to a 4mL glass tube with a tight screw top and add:

i. 0.5mL dH_2O

ii. 0.5mL 12N (37%) HCl

Mix i. and ii. before adding to sample glass tube

c. Put the samples in a heating chamber keeping 120°C overnight (~16 hours)

d. Let samples cool down to reach room temperature and dilute with 3mL dH_2O, giving a total volume of 4mL.

e. Samples are further diluted:

i. µL suspension: (225/Xmg sample/4mL))×5

ii. µL dH_2O: to a total of 4500µL

Use 7mL tubes with blue screw top.

Tissue concentration now is 0.25µg/ µL or 125µg dry tissue in 500µL suspension.

2. Reagents

a. Citric acid buffer:

50g Citric acid monohydrate ($C_6H_8O_7 \times H_2O,\ M_w = 210.14$)

12mL Acetic acid ($CH_3COOH,\ M_w = 60.05$)

120g Na-acetate trihydrate ($CH_3COONa \times 3\,H_2O$) or 72.37g Na-acetate without H_2O (M_w = 82.03)

34g Na-hydroxide ($NAOH,\ M_w = 40$)

Dissolve in dH_2O (Note: Hot. May alternatively be cooled on ice) and adjust (with dH_2O) to a total of 1 litre and pH to 6.0 (adjust with 1M or 5M NaOH or HCl).

Store at 4°C.

b. 3.15M Perchloric acid:

27mL 11.65M (70%) or 34.2mL 9.2M (60%) Perchloric acid ($HClO_4$, $M_w = 100.47$) is solved with dH_2O to a total volume of 100mL.

c. 0.05M Chloramine T:

1.41g Chloramine T ($C_7H_7ClNNaO_2S \times 3H_2O$, $M_w = 281.61$) (note: Chloramine T powder must be white)

20mL dH_2O

30mL Ethylene glycol monomethyl ether ($C_3H_8O_2$, $M_w = 76.10$)

50mL Citric acid buffer

Must be made freshly every time

d. 20% p-dimetylamino benzaldehyde (p-DABA):

20g p-DABA ($C_9H_{11}NO, M_W = 149{,}19$) (p-DABA,
Sigma art no. 156477-100G)

60mL Ethylene glycol monomethyl ether (VWR art no. 8.00857.1000)

Heat in 60°C water bath to dissolve, followed by a dilution with dH_2O to a total volume of 100mL. Cover with parafilm. Important: p-DABA precipitates when Ethylene glycol monomethyl ether cools or evaporates to a certain degree.

Must be made freshly every time

e. Stock hydroxyproline standard (0.1µg/µL, 250mL):

Solve 25mg Hydroxyproline in 250mL 10^{-3}N HCl (1N HCl diluted 1:1000)

Standards:

0µg/500µL test sample: 4000µL dH_2O

0.25µg/500µL test sample: 20µL stock + 3980µL dH_2O

0.50µg/500µL test sample: 40µL stock + 3960µL dH_2O

0.75µg/500µL test sample: 60µL stock + 3940µL dH_2O

1.00µg/500µL test sample: 80µL stock + 3920µL dH_2O

1.50µg/500µL test sample: 120µL stock + 3880µL dH_2O

2.00µg/500µL test sample: 160µL stock + 3840µL dH_2O

3. Analysis

All reagents should be room tempered before used in the analysis, with the exception of p-DABA that should be kept heated in a water bath until 5 minutes before adding to samples (to avoid precipitation). The analysis is time sensitive, which means that the sample tubes should be mixed in the same order and same time interval for every added reagent. Mix samples by gently shaking rack (avoid turning around). Use Multipipette with a 12.5mL tip to add reagents (250µL). Do not use hard plastic tubes (reacts with hot ethylene glycol), but soft plastic tubes (7mL). Do not use screw tops, but cover with parafilm (especially important before samples are put in the water bath). All samples and standards should be analyzed with two parallels.

Methodological procedure:

1. 500µL test sample/standard
2. 250µL Chloramine T

Mix and leave for 20 minutes in room temperature. Add thereafter:

3. 250µL 3.15M Perchloric acid

Mix and leave for 5 minutes (maximum 8 minutes). Then add:

4. 250µL 20% p-DABA

Mix and cover all samples with parafilm (colour reaction do not start before heated in water bath). Sample tubes are then put in a heated water bath, keeping 60±1°C, for 20 minutes, followed by quick cooling in a sink filled with cool water added ice cubes, for 5 minutes.

Read absorption spectrophotometrically at 557nm (use disposable plastic cyvettes)

The standard curve reflects hydroxyproline concentration in 125µg muscle tissue. Concentration is converted to collagen by multiplying with a factor of 6.94 (µg collagen/ µg hydroxyproline).

4. Hydroxyproline Standard Curves for the Determination of Total Collagen Content

Hydroxyproline standard curves using linear regression are shown below for the first (Figure A-1) and second (Figure A-2) analytical run:

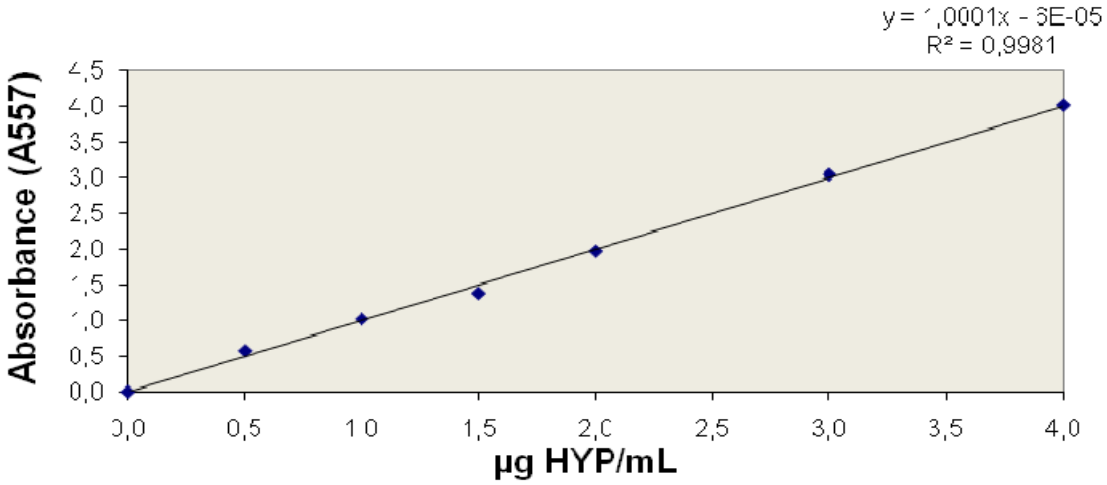

Figure A-1: Standard curve representing the first series of Hydroxyproline (HYP) analysis. Y-axis represents absorption measured at 557nm in arbitrary units (AU), whereas X-axis represents HYP concentration in µg/mL. Linear correlation coefficient reveals a linear relation ($R^2 = 0.9981$) between absorbency and concentrations ranging from 0.0 to 4.0µg HYP/mL. Y = 1.001x – 6E-05.

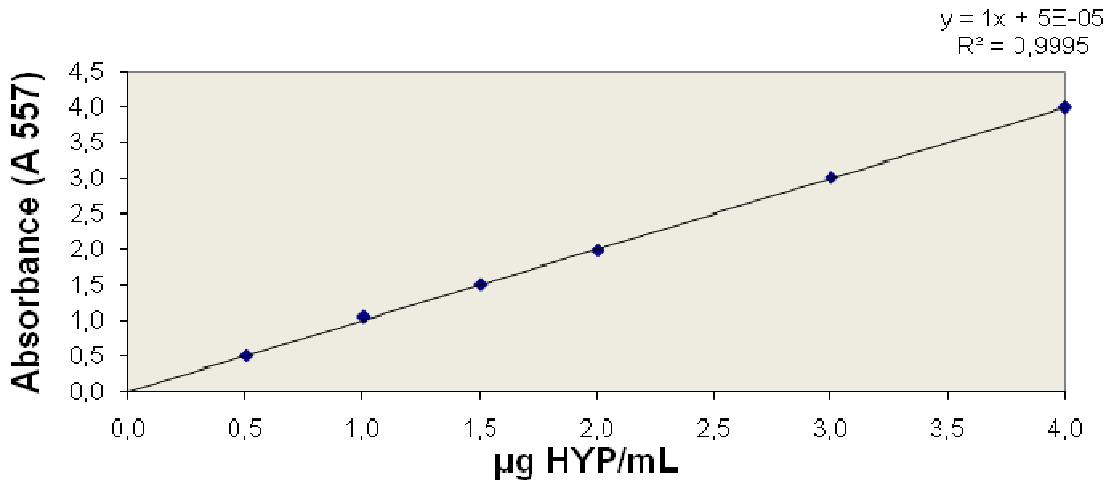

Figure A-2: Standard curve representing the second series of Hydroxyproline (HYP) analysis. Y-axis represents absorption measured at 557nm in arbitrary units (AU), whereas X-axis represents HYP concentration in µg/mL. Linear correlation coefficient reveals a linear relation ($R^2 = 0.9981$) between absorbency and concentrations ranging from 0.0 to 4.0µg HYP/mL. Y = 1x – 5E-05.

Appendix B

Selective Normative Data

Description	Normal limits	Unit
Respiration rate	70-150*	breaths/min
Heart rate	300-500*	beats/min
Body temperature	37.5-38.0*	°C
pH (whole blood)	7.40-7.44*	AU
pCO_2	33-41*	mmHg
pO_2	91-94*	mmHg
Haemoglobin	15.7*	g/dL
Glucose (fasting, venous)	3.2-5.0**	mmol/L
Hematocrit	0.41-0.51**	AU
Na^+	137-145**	mmol/L
K^+	3.6-4.6**	mmol/L
Ca^{++}	1.18-1.32**	mmol/L
Cl^-	98-106**	mmol/L
Total collagen (muscle)	0.4-4***	g/100g DW
Total collagen (lungs)	10-20***	g/100g DW

Sources:

* (64)

** (65) (Note: data representative for humans)

*** (15)

References

1. WHO. Cardiovascular Diseases. 2007 [100309]; Available from: http://www.who.int/mediacentre/factsheets/fs317/en/index.html.
2. WHO. The Atlas of Heart Disease and Stroke. 2009 [100309]; Available from: http://www.who.int/cardiovascular_diseases/resources/atlas/en/.
3. WHO. The Future. 2004 [100309]; Available from: http://www.who.int/cardiovascular_diseases/en/cvd_atlas_25_future.pdf.
4. Statistics Norway. Dødsfall etter årsak. Hele landet. 1991-2007 [080509]; Available from: http://www.ssb.no/dodsarsak/tab-2009-04-07-01.html.
5. Bragadeesh T, Jayaweera AR, Pascotto M, Micari A, Le DE, Kramer CM, et al. Post-ischaemic myocardial dysfunction (stunning) results from myofibrillar oedema. Heart. 2008 Feb;94(2):166-71.
6. Davis KL, Mehlhorn U, Laine GA, Allen SJ. Myocardial edema, left ventricular function, and pulmonary hypertension. J Appl Physiol. 1995 Jan;78(1):132-7.
7. Laine GA, Allen SJ. Left ventricular myocardial edema. Lymph flow, interstitial fibrosis, and cardiac function. Circ Res. 1991 Jun;68(6):1713-21.
8. Mehlhorn U, Davis KL, Burke EJ, Adams D, Laine GA, Allen SJ. Impact of cardiopulmonary bypass and cardioplegic arrest on myocardial lymphatic function. Am J Physiol. 1995 Jan;268(1 Pt 2):H178-83.
9. Pratt JW, Schertel ER, Schaefer SL, Esham KE, McClure DE, Heck CF, et al. Acute transient coronary sinus hypertension impairs left ventricular function and induces myocardial edema. Am J Physiol. 1996 Sep;271(3 Pt 2):H834-41.
10. Mehlhorn U, Geissler HJ, Laine GA, Allen SJ. Myocardial fluid balance. Eur J Cardiothorac Surg. 2001 Dec;20(6):1220-30.
11. Simonneau G, Galie N, Rubin LJ, Langleben D, Seeger W, Domenighetti G, et al. Clinical classification of pulmonary hypertension. J Am Coll Cardiol. 2004 Jun 16;43(12 Suppl S):5S-12S.
12. MacKenna DA, Vaplon SM, McCulloch AD. Microstructural model of perimysial collagen fibers for resting myocardial mechanics during ventricular filling. Am J Physiol. 1997 Sep;273(3 Pt 2):H1576-86.
13. Davis KL, Laine GA, Geissler HJ, Mehlhorn U, Brennan M, Allen SJ. Effects of myocardial edema on the development of myocardial interstitial fibrosis. Microcirculation. 2000 Aug;7(4):269-80.
14. Aukland K, Reed RK. Interstitial-lymphatic mechanisms in the control of extracellular fluid volume. Physiol Rev. 1993 Jan;73(1):1-78.
15. Aukland K, Nicolaysen G. Interstitial fluid volume: local regulatory mechanisms. Physiol Rev. 1981 Jul;61(3):556-643.
16. Soderhall C, Marenholz I, Kerscher T, Ruschendorf F, Esparza-Gordillo J, Worm M, et al. Variants in a novel epidermal collagen gene (COL29A1) are associated with atopic dermatitis. PLoS Biol. 2007 Sep;5(9):e242.
17. Nimni ME, Harkness RD. Molecular structure and functions of collagen. Nimni ME, editor. Boca Raton, FL: CRC Press, Inc.; 1988.
18. Byers PH, Click EM, Harper E, Bornstein P. Interchain disulfide bonds in procollagen are located in a large nontriple-helical COOH-terminal domain. Proc Natl Acad Sci U S A. 1975 Aug;72(8):3009-13.
19. Fessler LI, Morris NP, Fessler JH. Procollagen: biological scission of amino and carboxyl extension peptides. Proc Natl Acad Sci U S A. 1975 Dec;72(12):4905-9.
20. Veis A, Payne K. Collagen fibrillogenesis. Nimni ME, editor. Boca Raton, FL: CRC Press, Inc.; 1988.
21. Wiestner M, Krieg T, Horlein D, Glanville RW, Fietzek P, Muller PK. Inhibiting effect of procollagen peptides on collagen biosynthesis in fibroblast cultures. J Biol Chem. 1979 Aug 10;254(15):7016-23.
22. Comper WD, Laurent TC. Physiological function of connective tissue polysaccharides. Physiol Rev. 1978 Jan;58(1):255-315.

23. Tissot B, Ceroni A, Powell AK, Morris HR, Yates EA, Turnbull JE, et al. Software Tool for the Structural Determination of Glycosaminoglycans by Mass Spectrometry. Anal Chem. 2008 Oct 29.
24. Ikkos D, Luft R, Sjogren B. Distribution of fluid and sodium in healthy adults. Metabolism. 1954 Sep;3(5):400-4.
25. Levick JR. An Introduction to Cardiovascular Physiology. 4 th ed. ed. London: Hodder Arnold; 2003.
26. Starling EH. On the Absorption of Fluids from the Connective Tissue Spaces. J Physiol. 1896 May 5;19(4):312-26.
27. Berg A, Rubin K, Reed RK. [Beta1 integrins and edema formation in acute inflammation--new therapeutic possibilities?]. Tidsskr Nor Laegeforen. 2000 Oct 30;120(26):3142-6.
28. Aukland K. Local factors in the regulation of interstitial fluid volume (abstr.). Acta Physiol Scand Suppl. 1979;473(11).
29. Cho S, Atwood JE. Peripheral edema. Am J Med. 2002 Nov;113(7):580-6.
30. McDonald DM, Thurston G, Baluk P. Endothelial gaps as sites for plasma leakage in inflammation. Microcirculation. 1999 Mar;6(1):7-22.
31. Sun SC, Lie JT. Cardiac lymphatic obstruction: ultrastructure of acute-phase myocardial injury in dogs. Mayo Clin Proc. 1977 Dec;52(12):785-92.
32. Sasaguri S, Sunamori M, Saito K, Suzuki A. Early change of myocardial water during acute cardiac allograft rejection. Jpn Circ J. 1986 Nov;50(11):1113-9.
33. Laks H, Standeven J, Blair O, Hahn J, Jellinek M, Willman VL. The effects of cardiopulmonary bypass with crystalloid and colloid hemodilution on myocardial extravascular water. J Thorac Cardiovasc Surg. 1977 Jan;73(1):129-38.
34. Laine GA. Microvascular changes in the heart during chronic arterial hypertension. Circ Res. 1988 May;62(5):953-60.
35. Laine GA. Change in (dP/dt)max as an index of myocardial microvascular permeability. Circ Res. 1987 Aug;61(2):203-8.
36. Goddard CM, Allard MF, Hogg JC, Walley KR. Myocardial morphometric changes related to decreased contractility after endotoxin. Am J Physiol. 1996 Apr;270(4 Pt 2):H1446-52.
37. Miyamoto M, McClure DE, Schertel ER, Andrews PJ, Jones GA, Pratt JW, et al. Effects of hypoproteinemia-induced myocardial edema on left ventricular function. Am J Physiol. 1998 Mar;274(3 Pt 2):H937-44.
38. Pogatsa G, Dubecz E, Gabor G. The role of myocardial edema in the left ventricular diastolic stiffness. Basic Res Cardiol. 1976 May-Jun;71(3):263-9.
39. Rubboli A, Sobotka PA, Euler DE. Effect of acute edema on left ventricular function and coronary vascular resistance in the isolated rat heart. Am J Physiol. 1994 Sep;267(3 Pt 2):H1054-61.
40. Capasso JM, Robinson TF, Anversa P. Alterations in collagen cross-linking impair myocardial contractility in the mouse heart. Circ Res. 1989 Dec;65(6):1657-64.
41. Laine GA, Allen SJ, Katz J, Gabel JC, Drake RE. Outflow pressure reduces lymph flow rate from various tissues. Microvasc Res. 1987 Jan;33(1):135-42.
42. Wegria R, Zekert H, Walter KE, Entrup RW, De Schryver C, Kennedy W, et al. Effect of systemic venous pressure on drainage of lymph from thoracic duct. Am J Physiol. 1963 Feb;204:284-8.
43. Klein G, Schaefer A, Hilfiker-Kleiner D, Oppermann D, Shukla P, Quint A, et al. Increased collagen deposition and diastolic dysfunction but preserved myocardial hypertrophy after pressure overload in mice lacking PKCepsilon. Circ Res. 2005 Apr 15;96(7):748-55.
44. Rosenkranz S, Flesch M, Amann K, Haeuseler C, Kilter H, Seeland U, et al. Alterations of beta-adrenergic signaling and cardiac hypertrophy in transgenic mice overexpressing TGF-beta(1). Am J Physiol Heart Circ Physiol. 2002 Sep;283(3):H1253-62.
45. Weber KT, Brilla CG. Pathological hypertrophy and cardiac interstitium. Fibrosis and renin-angiotensin-aldosterone system. Circulation. 1991 Jun;83(6):1849-65.
46. Campbell SE, Katwa LC. Angiotensin II stimulated expression of transforming growth factor-beta1 in cardiac fibroblasts and myofibroblasts. J Mol Cell Cardiol. 1997 Jul;29(7):1947-58.
47. Overall CM, Wrana JL, Sodek J. Transcriptional and post-transcriptional regulation of 72-kDa gelatinase/type IV collagenase by transforming growth factor-beta 1 in human fibroblasts.

Comparisons with collagenase and tissue inhibitor of matrix metalloproteinase gene expression. J Biol Chem. 1991 Jul 25;266(21):14064-71.
48. Council of Europe. [100209]; Available from: http://conventions.coe.int/Treaty/EN/Treaties/PDF/123-Arev.pdf.
49. Nicklas W, Baneux P, Boot R, Decelle T, Deeny AA, Fumanelli M, et al. Recommendations for the health monitoring of rodent and rabbit colonies in breeding and experimental units. Lab Anim. 2002 Jan;36(1):20-42.
50. Brammer A, West CD, Allen SL. A comparison of propofol with other injectable anaesthetics in a rat model for measuring cardiovascular parameters. Lab Anim. 1993 Jul;27(3):250-7.
51. Stark RA, Nahrwold ML, Cohen PJ. Blind oral tracheal intubation of rats. J Appl Physiol. 1981 Nov;51(5):1355-6.
52. Waynforth HB, Flecknell PA. Experimental and surgical technique in the rat. 2 ed. Suffolk, UK: Elsevier Ltd.; 2004.
53. Woessner JF, Jr. The determination of hydroxyproline in tissue and protein samples containing small proportions of this imino acid. Arch Biochem Biophys. 1961 May;93:440-7.
54. Urashima T, Zhao M, Wagner R, Fajardo G, Farahani S, Quertermous T, et al. Molecular and physiological characterization of RV remodeling in a murine model of pulmonary stenosis. Am J Physiol Heart Circ Physiol. 2008 Sep;295(3):H1351-H68.
55. Nedrebo T, Karlsen TV, Salvesen GS, Reed RK. A novel function of insulin in rat dermis. J Physiol. 2004 Sep 1;559(Pt 2):583-91.
56. Desai KV, Laine GA, Stewart RH, Cox CS, Jr., Quick CM, Allen SJ, et al. Mechanics of the left ventricular myocardial interstitium: effects of acute and chronic myocardial edema. Am J Physiol Heart Circ Physiol. 2008 Jun;294(6):H2428-34.
57. Jia CX, Rabkin DG, Hart JP, Dean DA, Cabreriza SA, Weinberg AD, et al. Regional variation in myocardial water content in the edematous pig heart. J Surg Res. 2002 Jul;106(1):70-5.
58. Hamilton DL, Boyett MR, Harrison SM, Davies LA, Hopkins PM. The concentration-dependent effects of propofol on rat ventricular myocytes. Anesth Analg. 2000 Aug;91(2):276-82.
59. Cinel I, Gur S. Direct inotropic effects of propofol and adenosine on rat atrial muscle: possible mechanisms. Pharmacol Res. 2000 Aug;42(2):123-8.
60. Guenoun T, Montagne O, Laplace M, Crozatier B. Propofol-induced modifications of cardiomyocyte calcium transient and sarcoplasmic reticulum function in rats. Anesthesiology. 2000 Feb;92(2):542-9.
61. Riou B, Besse S, Lecarpentier Y, Viars P. In vitro effects of propofol on rat myocardium. Anesthesiology. 1992 Apr;76(4):609-16.
62. Sessler DI. Perioperative heat balance. Anesthesiology. 2000 Feb;92(2):578-96.
63. Bittar MN, Barnard JB, Khasati N, Richardson S. Should the pericardium be closed in patients undergoing cardiac surgery? Interact Cardiovasc Thorac Surg. 2005 Apr;4(2):151-5.
64. van Dongen JJ, Remie R, Rensema JW, van Wunnik GHJ. Manual of microsurgery on the laboratory rat. Huston JP, editor. Amsterdam, The Netherlands: Elsevier Science B.V; 1990.
65. Stakkestad JA, Åsberg A. Brukerhåndbok Klinisk Kjemi. 3 ed. Haugesund, Norway: Akademisk Fagforlag AS; 2004.